To appear in Astrophy. J. April 1, 2000 issue, Vol. 532

Modeling the Near-Infrared Luminosity Functions of Young Stellar Clusters

August A. Muench[1,2]

Department of Astronomy, University of Florida, Gainesville, FL 32611 and Harvard-Smithsonian Center for Astrophysics, Cambridge, MA 02138

gmuench@cfa.harvard.edu

Elizabeth A. Lada

Department of Astronomy, University of Florida, Gainesville, FL 32611

lada@astro.ufl.edu

and

Charles J. Lada

Harvard-Smithsonian Center for Astrophysics, Cambridge, MA 02138

clada@cfa.harvard.edu

ABSTRACT

We present the results of numerical experiments designed to evaluate the usefulness of near-infrared luminosity functions for constraining the Initial Mass Function (IMF) of young stellar populations. We test the sensitivity of the near-infrared K band luminosity function (KLF) of a young stellar cluster to variations in the underlying IMF, star forming history, and pre-main sequence mass-to-luminosity relations. Using Monte Carlo techniques, we create a suite of model luminosity functions systematically varying each of these basic underlying relations. From this numerical modeling, we find that the luminosity function of a young stellar population is considerably more sensitive to variations in the underlying initial mass function than to either variations in the star forming history or assumed pre-main-sequence (PMS) mass-to-luminosity relation. Variations in a cluster's star forming history are also found to produce significant changes in the

[1]Smithsonian Predoctoral Fellow

[2]present address: Harvard-Smithsonian Center for Astrophysics, 60 Garden Street, Mail Stop 42, Cambridge, MA 02138 USA

KLF. In particular, we find that the KLFs of young clusters evolve in a systematic manner with increasing mean age. Our experiments indicate that variations in the PMS mass-to-luminosity relation, resulting from differences in adopted PMS tracks produce only small effects on the form of the model luminosity functions and that these effects are mostly likely not detectable observationally.

To illustrate the potential effectiveness of using the KLF of a young cluster to constrain its IMF, we model the observed K band luminosity function of the nearby Trapezium cluster. With knowledge of the star forming history of this cluster obtained from optical spectroscopic studies, we derive the simplest underlying IMF whose model luminosity function matches the observations. Our derived mass function for the Trapezium spans two orders of magnitude in stellar mass ($5 > M_{\odot} > 0.02$) and has a peak near the hydrogen burning limit. Below the hydrogen burning limit, the mass function steadily decreases with decreasing mass throughout the brown dwarf regime. Comparison of our IMF with that derived by optical and spectroscopic methods for the entire Orion Nebula Cluster suggests that modeling the KLF is indeed a useful tool for constraining the mass function in young stellar clusters particularly at and below the hydrogen burning limit.

Subject headings: infrared: stars — stars: low-mass, brown dwarfs — stars: luminosity function, mass function — stars: pre-main sequence

1. Introduction

The development of sensitive, large format imaging arrays at near-infrared wavelengths has made it possible to obtain statistically significant and complete samplings of the near-infrared luminosity functions of very young embedded clusters. In principle such luminosity functions should provide fundamental constraints on the stellar initial mass function (IMF)[1] of these clusters and its possible variation in space and time. There are several advantages and disadvantages in using young embedded clusters to study issues of the initial mass function (for a summary see Lada, Lada & Muench (1998); Lada (1999)). The biggest advantage of studying the luminosity functions of very young clusters is that the low mass stars in these clusters are brighter than at any other time in their evolution. Consequently modern NIR detectors even on modest telescopes can completely sample the entire IMF of nearby (D < 1 Kpc) embedded clusters down to and *well below* the hydrogen burning limit. However, the youth of the clusters also makes interpreting the luminosity functions of these clusters, in terms of an IMF, difficult, since most members are still in the pre-main sequence phase of their evolution. For pre-main sequence stars, there is no unique mass to

[1]In all cases we will refer to the mass function not the mass spectrum of stars. The mass function is the number of stars per unit volume per unit *log mass*. The Salpeter (1955) mass function would be a power-law $\xi(\log(m_\star)) = m^\Gamma$ with a index $\Gamma = -1.35$ in this definition.

luminosity relation and consequently one must rely on using evolutionary models to understand the underlying IMFs of embedded clusters.

Various groups have modeled the luminosity functions of young clusters using realistic stellar mass functions and appropriate mass-luminosity relationships (e.g., Zinnecker et al., (1993); Strom, Strom & Merrill (1993); Fletcher & Stahler (1994a); Lada & Lada (1995); Meageth (1996)). Zinnecker, McCaughrean & Wilking (1993) were the first to present model KLFs of very young clusters. For their model clusters they adopted a "coeval" star formation history in which all the stars were formed at a single instant of time. Moreover, they assumed blackbody radiation to derive bolometric corrections and assumed a single form for the IMF. Consequently, their models were not very realistic and they did not attempt to fit or directly compare their models to observed KLFs. Lada & Lada (1995) (LL95, hereafter) improved on this work by developing evolutionary models for the KLFs of young clusters ranging in age from 10^6 to $< 10^7$ yrs, using empirically determined bolometric corrections and allowing for non-coeval or continuous star formation in the clusters. Moreover, they directly compared their models to observed KLFs of young clusters. However, similar to the Zinnecker et al. work, Lada & Lada assumed a single underlying IMF (i.e., the Miller & Scalo (1979) field star IMF) and employed the published pre-main sequence evolutionary tracks of D'Antona & Mazzitelli (1994). In addition, their model KLFs were constructed for stars having masses between 0.1 and 20 $M_{\odot}$, since the existing PMS tracks did not extend below 0.1 $M_{\odot}$. Thus their results are only valid as long as there are no, or at least very few, brown dwarfs in these clusters. Their modeling efforts produced several interesting results. For example, Lada & Lada found that for a fixed IMF the shape of a cluster KLF depends primarily on the duration of star formation and age of the cluster and that in general the KLFs broaden with age.

It is somewhat difficult to evaluate the success of the early modeling work to constrain the IMF of embedded clusters because: 1) these early models typically employed one set of PMS tracks with stellar masses greater than 0.1 $M_{\odot}$; 2) the models only considered one fixed IMF and, 3) the ages and age spreads of the clusters were not well constrained. Fortunately, improvements in these areas have recently been made. For example, PMS evolutionary tracks have been extended to objects with masses well below the hydrogen burning limit. In addition, improved age estimates for several clusters such as the Trapezium (Hillenbrand 1997) and IC 348 (Herbig 1998) have been made.

Given these advances, we have extended the earlier modeling work and have developed a new suite of KLF evolutionary models. These new models are based on Monte Carlo techniques and are a considerable improvement over the earlier calculations. In particular, the new models incorporate improved bolometric corrections and new PMS tracks, thereby including objects with masses below the hydrogen burning limit. In this paper, we describe our new models and present our results from this modeling effort. In addition, we investigate the utility of using near-infrared luminosity functions for interpreting and constraining the IMF of young embedded stellar clusters. Since the observed luminosity function of a young cluster depends not only on the underlying IMF, but also the pre-main sequence mass-to-luminosity relation and the star forming history of the clusters, it is important to understand how changes in the pre-main sequence mass-to-luminosity

relations, star forming history and the underlying IMF affect the resulting KLF. Therefore, we have systematically varied each of these three basic underlying inputs and have evaluated the sensitivity of the KLF to each input. Finally, we illustrate the effectiveness of using the KLF of a young cluster to constrain its IMF by modeling the KLF of the Trapezium cluster for which detailed knowledge of its star formation history is known from optical spectroscopic studies (Hillenbrand 1997).

2. Modeling the Luminosity Function

The observed luminosity function (LF) for a young cluster depends on the pre-main sequence mass to luminosity (M-L) relation, the star forming history (SFH) of the cluster and the cluster's underlying initial mass function (IMF). We constructed model K-band LFs (KLFs) for a suite of synthetic young clusters using varying PMS M-L relations, SFHs and IMFs. We first specified a functional form for the SFH and the IMF for each synthetic cluster. The ages and masses of the individual cluster members were then sampled from these adopted functions using a Monte Carlo rejection method algorithm. We derived the monochromatic magnitudes for each model star from its age and mass by using theoretical pre-main sequence evolutionary models and empirical bolometric corrections taken from the literature. For each synthetic cluster, we binned the resulting magnitudes in half magnitude bins to compare to observed cluster luminosity functions. Our standard cluster contained 1000 stars and for each SFH and IMF we produced 100 independent luminosity functions. We computed the mean luminosity function from these 100 realizations, and report the one sigma standard deviation of the computed mean.

For the models presented in this paper, we assumed a constant star formation rate over the SFH of the cluster. We parameterized the SFH using a "mean age", τ, and an "age spread", $\Delta\tau$. For example, a coeval cluster will have no age spread and $\Delta\tau/\tau = 0.0$. A cluster with the largest possible age spread would have $\Delta\tau/\tau = 2.0$ with star formation starting $2 \times \tau$ years ago and continuing to the present. Figure 1 illustrates these definitions. Our model SFH then approximates any SFH to first order by using the most common age of the members and a rough age spread.

In our standard model, stars have masses from 80 to 0.02 $M_\odot$. For all the models considered here, the youngest ($1 - 5 \times 10^5$ years) cluster members with masses greater than 5 $M_\odot$ will have already reached the Zero Age Main Sequence (ZAMS). For these massive stars, we converted their age and mass to bolometric luminosity and effective temperature using a theoretical ZAMS derived from Schaller et al., (1992). Between 1 and 5 $M_\odot$, we used pre-main sequence evolutionary models from either Palla & Stahler (1993) or Bernasconi (1996a). For stars below 1 $M_\odot$ and brown dwarfs, we used PMS evolutionary models from D'Antona & Mazzitelli (1994,1998). Appendix B describes how these three regimes were combined. Using the bolometric luminosity and effective temperatures derived from these stellar models, we converted to an absolute magnitude using the formula:

$$M_\lambda = M_{bol,\odot} - 2.5 \times \log(L/L_\odot) - BC_\lambda(T_{eff}) \quad (1)$$

Our empirical bolometric corrections were tabulated as functions of effective temperature and were taken from the literature. In addition, we assumed $M_{bol,\odot} = 4.75$. We list the sources of the bolometric corrections in Appendix A.

For the purposes of this paper, we will only present an analysis of the K-band (2.2 μm) luminosity functions for our model stars, though any monochromatic luminosity functions could be calculated. Note that our models did not include the effects of excess infrared flux due to unresolved binaries or circumstellar accretion disks around PMS stars. However, by choosing relatively wide (half magnitude) bins for the luminosity function, we can minimize the variable effects of infrared excess flux. The model KLFs for our young clusters did not include the effects of differential interstellar extinction common in young star forming regions. We did not include protostars in our luminosity function models since the contribution of proto-stellar objects to the luminosity function of most star forming regions should be small (Fletcher & Stahler 1994a,b). Finally, we defined our input mass function as a single star mass function.

3. Experiments

3.1. Evolutionary Pre-Main Sequence Models

The evolution of pre-main sequence (PMS) stars across the HR diagram and onto the main sequence is not observationally well constrained. Details of PMS evolution rely heavily upon theoretical PMS models. These theoretical PMS models vary in their predictions depending on the numerical methods and theoretical assumptions used in their creation. Since these PMS models are used to convert from a stellar age and mass to a monochromatic magnitude, the resulting luminosity functions will depend to some degree on the PMS evolutionary models which are chosen. To evaluate how PMS models with different input physics, chemical abundances or effective mass ranges affect the shape and form of a model luminosity function, we constructed and compared model luminosity functions calculated assuming different PMS models.

For these experiments, we fixed the initial mass function to have a log-normal distribution:

$$\xi(\log(\frac{M}{M_\odot})) \quad = \quad c1 * \exp(-c2 * (\log(\frac{M}{M_\odot}) - c3)^2)), \tag{2}$$

where c1 is a normalization constant, c2 equals $1/(2\log(\sigma)^2)$, c3 equals $\overline{log(\frac{M}{M_\odot})}$ or the mean log mass of the distribution, and σ is the variance of this mean. The mean and variance that we adopted correspond to the field star mass function given by Miller & Scalo (1979) (MS79, here after), having constants of c2 = 1.09 and c3 = −1.02 or a mean mass of 0.0955 $M_\odot$. We produced a suite of model clusters with a range of mean ages from 0.2 to 15 Myrs and age spreads from coeval to twice the mean age of the model cluster. For the purposes of evaluating the effects of using different input PMS models, we only directly compared KLF models having identical star forming histories.

3.1.1. D'Antona & Mazzitelli (1994): Differing Input Physics

D'Antona & Mazzitelli (1994) (hereafter DM94) calculated four different sets of evolutionary PMS models varying two input physical parameters, the input opacity tables and the treatments of internal convection. Table 1 summarizes the four combinations of input physics and other parameters of the DM94 PMS models. Only one of these data sets contained stars with masses less than the hydrogen burning limit. Consequently, we used a common range of stellar masses from 2.5 to 0.1 $M_\odot$ to compute different model KLFs using the four sets of DM94 PMS models. Figure 2 compares synthetic KLFs computed from the DM94 PMS models for coeval models with mean ages of 1 and 7 million years, respectively. In Figure 2, different symbols correspond to different input opacity tables in the PMS models used. For the 1 million year coeval models, the two KLFs corresponding to PMS models with Kurucz opacities are essentially indistinguishable, indicating that the KLFs are insensitive to the convection model used. The two model KLFs corresponding to PMS models with Alexander opacities exhibit a relatively narrow but significant feature or peak between $M_K \sim$ 3-4 which is not apparent in the KLFs with Kurucz opacities. The position of this spike is different for the two convection models used with the Alexander opacities. This feature is due to deuterium burning which causes a slowing of the stellar luminosity evolution (Zinnecker et al., 1993) and therefore results in a pile up of stars in the luminosity function. The deuterium burning spike is absent in the 7 Myr coeval model in Figure 2, and in all coeval models with mean ages greater than 2-3 Myrs for stars above the hydrogen burning limit. The onset of deuterium burning is a function of stellar mass. Low mass stars contract more slowly than higher mass stars and begin burning deuterium after high mass stars. However by 3 Myrs, even stars at the hydrogen burning limit would have burned all of their initial deuterium abundance.

A second feature of interest in the KLFs is the spike/dip at $M_K = 2$ in the 7 Myr coeval model. It is present in all four 7 Myr KLFs and in all KLFs with mean ages greater than 3-4 Myr. This feature is the result of stars reaching a luminosity maximum on radiative tracks before beginning hydrogen burning and moving to lower luminosities on the main sequence (Iben 1965). We refer to this feature as the luminosity maximum spike (LMS). The luminosity maximum spike has been studied by Belikov & Piskunov (1997) in intermediate age (50-100 Myrs) clusters and these authors have used it to study the age of the Pleiades open cluster (Belikov et al., 1998).

Model KLFs appear degenerate in the absence of the deuterium burning spike. The existence of a deuterium spike removes the degeneracy and differentiates between the two different PMS opacity models. Moreover, the position of the deuterium burning spike can differentiate between the two convection treatments but only for Alexander opacities. However, only the youngest clusters exhibit a deuterium burning spike. Model KLFs computed with different PMS tracks and with mean ages greater then 2-3 Myrs are essentially indistinguishable from each other and consequently insensitive to the input physics of the PMS models. Note that the deuterium burning spike is most prominent when deuterium burning occurs in those stars with masses at the peak of the chosen IMF, which for models discussed here occurs at the hydrogen burning limit (mean ages 1-2 Myrs).

Introducing an age spread to the cluster star forming history diminishes the differences between the KLFs for all four DM94 and at any cluster mean age. While we fully describe the effects of age and age spread on the model KLFs in section 3.2, these result implies that except in the youngest clusters, the KLF will be observationally insensitive to variations in the input physics of the PMS models.

To further study how different PMS models affect the model KLFs, we compared the PMS models of DM94 with the more recent and improved calculations of D'Antona & Mazzitelli (1998) (DM98). Table 1 lists the relevant characteristics of the DM98 models. We constructed model KLFs computed with the standard mass range (0.02 to 80 $M_{\odot}$) using the DM94 ACM and DM98 d2.5 PMS models. These two PMS models have similar deuterium abundances but DM98 have advancements to the opacity table and treatment of convection as well as a new equation of state. Figure 3 compares model KLFs using these two PMS models with a coeval cluster SFH and mean ages of 0.8 and 5 million years. In general the overall shapes of the model KLFs from the two different PMS models are quite similar but some minor differences can be quantified. First, the DM98 model KLFs are somewhat narrower and have peaks shifted to slightly brighter magnitudes than those KLFs corresponding to the DM94 ACM model. This was a consistent result for all cluster ages and star forming histories. Second, the largest differences between the model KLFs occur at the faint end. This is where DM98 describe the largest differences in their PMS models with respect to the DM94 PMS models. DM98 PMS models have a very different resulting mass-effective temperature relation for low mass stars and brown dwarfs than DM94. Since the K band bolometric correction is fairly insensitive to effective temperature for stars cooler than 3500K (see Appendix A), these changes do not radically affect the model KLF. Further, DM98 PMS models have larger luminosities for the low mass stars and young brown dwarfs compared to DM94. Likewise the DM98 model KLFs are shifted to brighter magnitudes with respect to DM94 for the faint end of the KLF. However, these differences in the KLFs are relatively small and it would be difficult, observationally, to distinguish between them.

3.1.2. D'Antona & Mazzitelli (1998): Variations in Deuterium Abundance

The DM98 PMS models were specifically created to study the effects of varying the initial deuterium abundance for PMS evolutionary calculations. It is unclear how much deuterium pre-main sequence stars might contain as they evolve from the birthline toward the main sequence. And there is little observational evidence to constrain this parameter, so it should be considered as an ambiguity in modeling the KLFs. We studied the effects of the deuterium abundance on the KLFs by experimenting with the three PMS models presented by DM98. The opacities used by DM98 in their PMS models are advancements to those in the DM94 PMS models which produced a deuterium burning spike in the KLFs of Figure 2. DM98 input physics and deuterium abundances are summarized in Table 1. We produced model KLFs using the three DM98 PMS models, d1.5, d2.5, and d4.5, so labeled by their respective deuterium abundance ratios, e.g., model d1.5 equals

a deuterium abundance of 1.0×10^{-5}. Respectively, these three PMS models have deuterium abundances of one half, one and two times the interstellar deuterium abundance, which is $[D/H]_0 = 2.0 \times 10^{-5}$. Figure 4 compares model KLFs derived from these PMS models for mean ages of 2 and 7 Myr and both coeval and $\Delta\tau/\tau = 2.0$ age spreads. Comparing the coeval models it is clear that increasing the [D/H] abundance shifts the deuterium burning spike to brighter magnitudes and increases its size. The deuterium burning peak disappeared from the d1.5 KLF by 3 Myr, the d2.5 KLFs by 10 Myr and from the d4.5 KLFs not until beyond 10 Myr. For model KLFs shown in Figure 4 with the maximum age spread, variations in the KLFs due to changes in the initial deuterium abundance are too small to be observable. The main result here is that variations in the $[D/H]$ ratio only produce significant (i.e., observable) differences in the model KLFs of coeval (no age spread) clusters. For these clusters variations in deuterium abundance affects the location and size of the deuterium burning feature and this occurs only in younger ($\tau < 3$ Myr) clusters or for the highest deuterium abundances. Once stars have undergone deuterium burning, their KLFs are identical. Again, the presence of an age spread dilutes the deuterium burning feature rendering the form of the cluster KLF independent of the $[D/H]$ ratio.

3.1.3. Effective Mass Ranges for PMS Models

We investigated the effects of using different IMF mass ranges by comparing model KLFs with the standard mass range (0.02 to 80 $M_\odot$) to model KLFs with a truncated mass range (0.1 to 2.5 $M_\odot$), i.e., one excluding brown dwarfs, intermediate or high mass stars. This experiment is useful for comparing our model LFs to prior LF modeling by other authors who typically did not include stars below the hydrogen burning limit or did not include high mass stars. Figure 5 compares model KLFs with truncated and standard mass ranges for two different star forming histories. For a coeval SFH (upper panel, mean age 3.0 Myr), a truncation in the mass range produces a truncation in the model KLFs at the highest and lowest magnitude bins. However, with an age spread (lower panel, same mean age, $\Delta\tau/\tau = 2.0$), the truncated model KLF is deficient in stars over a wider range of magnitudes, and the two KLFs are similar only over a narrow range of magnitudes. The form of the cluster KLF is clearly very sensitive to the adopted mass range of the underlying IMF.

3.2. Star Formation History

As shown in the experiments of sections 3.1.1 and 3.1.2, mean age and age spread have an important effect on the KLF. To more fully explore this, we created model KLFs with a range of mean ages and age spreads, using a single underlying mass function, and a fixed set of PMS tracks. For these experiments, we used the same IMF as in section 3.1 (see equation 2). As in the previous section, we considered two mass ranges for the IMF, one range with stars down to the 0.1 $M_\odot$ and one including brown dwarfs with masses down to 0.02 $M_\odot$. We adopted a PMS evolutionary model that is our standard combination of DM98 d2.5 PMS models, Bernasconi (1996a) intermediate-

mass PMS models, and Schaller et al., (1992) ZAMS models (see Appendix B). We compared the effects of changing the mean age and age spread by studying how model KLFs evolve with time.

Figure 6 compares model KLFs with different mean ages and cluster age spreads. Each panel simultaneously displays a one, three and ten million year mean age cluster KLF for a specific $\Delta\tau/\tau$. For a given age spread, the models clearly shift to fainter magnitudes with increasing mean age. For small age spreads, the deuterium burning feature also evolves to fainter magnitudes with time appearing at $M_K = 3.5$ at 1 Myrs and $M_K = 5.5$ at 3 Myrs, and $M_K = 8$ at 10 Myrs. To quantify the KLF evolution with time, we calculated the mean K magnitude of the model KLF at each mean age from 0.5 to 10 Myrs and for a range of age spreads. In Figure 7, we plot the KLF mean magnitude versus the cluster mean age. Also we show this value for the two limiting values of $\Delta\tau/\tau$. Two sets of curves are plotted, the upper corresponding to an underlying cluster IMF with brown dwarfs (standard IMF) and the lower to an underlying IMF having no stars with masses less than 0.1 $M_\odot$.

The mean K magnitude of the model KLFs evolves over 2 magnitudes in the first 10 Myrs of the cluster lifetime, regardless of the age spread or the mass range over which the IMF was considered. Age spread has little effect except to slightly shift the KLFs to brighter magnitudes. The evolution of the mean K magnitude proceeds most quickly in the first 3 million years where the models evolve by 1 full magnitude. The model KLFs without brown dwarfs naturally have significantly brighter mean values but for these KLFs the mean K magnitude evolves similarly to the standard models. This indicates that the KLFs are more sensitive to changes in the underlying IMF than to changes in the cluster star forming history. We also studied the width of the model KLFs and found that KLFs widen systematically with time as was shown by LL95.

Variations in the mean cluster age produce more significant changes in the the model KLFs than do changes in the cluster age spread. We show in Figure 8, model KLFs for two mean ages and for both of these mean ages we show the four different age spreads from Figure 6. For a given mean age, it would be difficult to observationally distinguish clusters with differing age spreads. In detail, models with differing age spreads do exhibit differences in the prominence of the deuterium burning spike and the maximum luminosity dip/spike. At what point can one distinguish a coeval model KLF from a model KLF with an age spread? To answer this question, we compared model KLFs with increasing age spread to a coeval model of the same mean age. Using the χ^2 test, we distinguished the age spread at which the models KLFs no longer appear to be coeval. The general trend from our test is that for an increasing mean age, we require a steadily increasing age spread to distinguish the models from a coeval KLF. For mean ages up to 5 Myrs, a cluster KLF appears coeval until the duration of star formation equals the age of the cluster. Between 5 and 10 Myr mean ages, the deuterium burning feature is present among the brown dwarfs but is not very prominent in the model KLFs. Only a very small age spread is required to erase it from the model KLFs and the models no longer appear "coeval" with only a small amount of age spread. Once the deuterium burning feature is lost from the M-L relation, the models require very large and probably unrealistic age spreads for them to significantly differ from a coeval model of the

same mean age.

3.3. Initial Mass Function

We varied the underlying initial mass function of a young cluster to test the influence of the input IMF on the model KLFs. In previous sections we used a single IMF equivalent to the log-normal (MS79) mass function and only changed the mass limits to this IMF. To test the sensitivity of the KLF to variations in the underlying IMF, we adopted a simple two power-law IMF characterized by the form:

$$\xi(\log m_\star) \quad = \quad A \times m_\star^\Gamma \tag{3}$$

for each power-law segment. We used the symbol Γ to represent the power-law index of the mass function. Two power-law segments are joined at a mass, m_{break}. The power-law index for masses greater than some m_{break}, is Γ_1. For masses below the m_{break} value, the IMF index is Γ_2. Figure 9 illustrates and compares a sample of the mass functions we used. The log-normal IMF shown is that used in sections 3.1 and 3.2 and follows the MS79 parameterization. The example two power-law IMFs shown in Figure 9 have $\Gamma_1 = -1.35$, $m_{break} = 0.5\ M_\odot$ and Γ_2 varying from -1.35 to +1.0.

In these experiments, we varied Γ_1 values from -2.5 to -0.25, m_{break} from 0.06 to 1.5 $M_\odot$ and Γ_2 values from -1.35 to +2.0. Figure 10 displays some of the model KLFs and the corresponding underlying IMFs. The cluster star forming history used for these models has a mean age of 5 Myrs and a $\Delta\tau/\tau = 1.0$, or an age spread of 5 Myrs. We show model KLFs normalized to the bright end of the KLF where the underlying IMF power-law indices have identical Γ_1 slopes equal to -1.35. This example uses a $m_{break} = 0.5 M_\odot$ and five Γ_2 values equal to -1.35, -0.40, 0.0, +0.40 and +1.35. The most steeply rising KLF corresponds to a single Salpeter (1955) power-law IMF over the entire standard mass range.

Model KLFs display variations due to changes in all three parameters of the two power-law IMF. In Figure 10, the effects of changing Γ_2 are large and the differences between KLFs with a slightly rising and a slightly falling IMF below the m_{break} are significant. Varying the m_{break} produces shifts in the peak of the model KLFs. Another result of these tests is that over the range of K magnitudes governed by a single underlying IMF power-law, the model KLF tends to be characterized by a power-law like slope.

This is true both for the bright and faint slopes of the model KLFs away from the turnover caused by the m_{break} in the model IMF. However, we do note that features (e.g., peaks or dips) can arise in the LF of a cluster which do not correspond to features in the underlying Mass Function, but instead, result from changes in the slope of the Mass-Luminosity relation (Mazzitelli 1972; D'Antona & Mazzitelli 1983; Kroupa, Tout, & Gilmore 1993). Such a feature is present at $M_K = 5.5$ in the model KLFs of Figure 10 and this peak is the result of a change of slope in the Mass-Luminosity relation due to deuterium burning. This small peak is not related to a

corresponding feature in the underlying Mass Function. Moreover, it is quite small and is not likely to be observationally detectable (see Section 3.1). In addition, the steep downward trend often seen in the last bin of the model KLFs is the result of truncating the mass range for the underlying IMF at 0.02 $M_{\odot}$, which is the lower mass limit of the model Mass-Luminosity relation.

In summary, these calculations clearly show that the shape of the model KLF is very sensitive to variations in the underlying cluster IMF. Indeed, modest variations in the cluster IMF produce significantly greater responses in the model KLFs than do variations in the SFH and PMS model input physics.

4. Discussion

4.1. Results and Implications of Numerical Experiments

From these numerical experiments which evaluate the sensitivity of the K-band luminosity function to variations in three of its fundamental physical parameters: its underlying IMF, its star forming history, and its mass-to-luminosity relation, we find that the KLF of a young cluster is more sensitive to variations in its underlying IMF than to either variations in the star forming history or the PMS mass-to-luminosity relation.

We also find that variations in the cluster mean age can produce a significant response in the KLF of a young cluster. In particular, we find that the KLF systematically evolves with time. Both the mean magnitude and the width of the KLF increase with increasing mean age, confirming the results of earlier modeling (LL95). At the same time, variations in the cluster age spread are found to have a small effect on the form of the KLF and would likely be difficult to distinguish observationally.

Except for the youngest and purely coeval clusters, we find that the synthetic KLFs appear relatively insensitive to the adopted PMS evolutionary models (at least for the range of PMS models considered here). In the youngest coeval clusters, the location and size of the deuterium burning spike in the KLF was found to depend sensitively on the PMS tracks adopted for the underlying stars. However, we find that even a small amount of age spread broadens the spike and would make it observationally difficult to detect.

We conclude from these experiments that the KLF of a young stellar population can be used to place interesting constraints on the form of the cluster's underlying IMF, provided an independent estimate of the cluster mean age is available. The most direct method of determining the mean age of a young cluster is to obtain optical or infrared spectra and place the objects on the HR diagram. Through comparison to theoretical PMS tracks, the ages of the stars are determined and a mean age for the cluster derived.

From spectroscopic observations, one can also simultaneously derive the individual masses of

the stars and with complete spectra for all cluster members, an independent and more direct determination of the IMF results. However because of spectroscopic sensitivity limits, the determination of masses is usually only possible for the bright stellar population. Since the monochromatic K magnitude of the cluster members can be acquired for stars much fainter than the limit of spectroscopic methods, the analysis of the NIR luminosity function is a particularly powerful tool for investigating the IMF of faint stars in distant clusters or stars at and below the hydrogen burning limit in nearby clusters. Determining the fraction of cluster members at and below the hydrogen burning limit is a holy grail of present stellar research. The application of the luminosity function method to a nearby populous cluster would provide a first glimpse into the brown dwarf population formed at the time of a typical open cluster's birth.

4.2. Comparing Models with Observations: The Trapezium Cluster

The Trapezium cluster is a excellent system for evaluating the KLF modeling techniques developed in this paper. It is the most densely populated and best studied nearby (D $\sim$ 400-450pc) cluster, and the central part of a much larger cluster known as the Orion Nebula Cluster (ONC). The ONC has recently been studied by Hillenbrand (1997), who used optical spectroscopy to obtain a mean age for the cluster of 0.8×10^6 years and to construct an IMF for stars with masses primarily in excess of the hydrogen burning limit (HBL). In addition, infrared imaging surveys have been made of both the Trapezium cluster (Zinnecker et al., 1993; McCaughrean et al., 1995) and the ONC (Ali & DePoy 1995) enabling the construction of the cluster KLF. For comparison with our models, we consider only the KLF for the Trapezium cluster, the 5' by 5' central core of the ONC.

We constructed a KLF of the Trapezium by combining the published KLFs of Zinnecker et al., (1993) and McCaughrean et al., (1995). Our adopted KLF for the Trapezium is shown in the top panel of Figure 11. The Zinnecker et al. KLF includes the bright stars but is not complete at and below the HBL. The McCaughrean et al. KLF extends to very faint magnitudes, well below the HBL for a one million year old cluster, 400 pc distant, but because of source saturation, is incomplete for and does not include bright stars. Neither of these referenced cluster KLFs were corrected for contamination by foreground or background field stars. In addition, neither was corrected for the effects of nebular contamination which would confuse the completeness of the surveys. However, we compared this combined Trapezium KLF to the KLF from the Ali & DePoy (1995) survey of the ONC and found good agreement in the location of the turnover, bright and faint ends of the two KLFs, although the Ali & Depoy survey was not as sensitive as that represented by the McCaughrean et al. KLF. We reiterate that the extent to which the combined KLF represents the true Trapezium KLF is uncertain because we cannot account for field star or nebular contamination.

Here our goal is to find the simplest functional from of an underlying IMF whose resulting model KLF will best fit the observed KLF. We constrained the star forming history of the Trapezium cluster by using the mean age from Hillenbrand (1997) i.e., 0.8 million years. We allowed an age

spread of 1.2 million years ($\Delta\tau/\tau = 1.5$) about this mean age, corresponding to constant star formation from 0.2 to 1.4 million years ago. We inspected the observed KLF and determined that a single power law IMF could not satisfy the observations since the KLF has a peak and turnover well above the completeness limits of the two surveys. Therefore we began with a simple 2 power law IMFs. We next used a three power law IMF with a flat (zero slope) IMF in the middle. For symmetry, the two outer power-law slopes were set to have equal but opposite sign slopes. We varied these outer slopes to have absolute values between 0.25 and 2.00 and adjusted the mass range over which the middle slope of the IMF was flat. Finally as a third set of experiments, we allowed the slope of the middle power law to vary, still holding the outer two slopes to have equal but opposite sign slopes.

We produced a suite of model KLFs for these different IMFs and compared them to the combined Trapezium KLF using a chi-square fitting procedure. Simply, we normalized model KLFs to the observed KLF such that the model and observed KLFs contain the same number of stars between absolute K magnitudes of 0 and 6.5. We then calculated the χ^2 statistic and probability over this K magnitude range. To derive a best fit, we compared a suite of model KLFs varying a single IMF parameter, e.g, the middle slope or one of the m_{break} values and then determining the χ^2 minima for that variable. Model KLFs were created for a range of possible IMF parameters and compared to the Trapezium KLF in this way.

Best fit model IMFs for each of the tested functional forms of the IMF are listed in Table 2. Two power law fits in general were not good. Symmetric flat topped IMFs fit better and finally a slightly rising IMF across the middle provided a best fit with $\chi^2 \sim 1$. Some variation in each of the parameters still allowed for a fit of $\chi^2 \sim 1$ and examples are listed in Table 2. The IMFs f and g produced best fits to the data: For purposes of discussion, we adopt IMF (g) as representative of the Trapezium IMF and repeat its parameters here:

$$\Gamma = \begin{cases} +1.35 & : \quad 0.08\,M_\odot > M_\star \\ -0.25 & : \quad 0.80\,M_\odot > M_\star > 0.08\,M_\odot \\ -1.35 & : \quad M_\star > 0.80\,M_\odot \end{cases} \tag{4}$$

The model KLF corresponding to IMF (g) is shown in the top panel of Figure 11 compared to the combined Trapezium KLF and compared to a model KLF calculated with the single power law slope Salpeter (1955) field star IMF over the entire standard mass range.

From our modeling of the observed KLF for the Trapezium cluster we find that the predicted IMF has a rising slope for intermediate mass stars, flattens around a solar mass, reaches a peak near the HBL and turns over below the hydrogen burning limit. There are several comparisons between the observed and modeled Trapezium KLF and between the ONC IMF derived by Hillenbrand and our derived IMF (g) which should be made. First, there exists a significant "tail" to the observed Trapezium luminosity function which is not accounted for in the model KLFs. No attempt was made to account for these very faint stars as cluster members because if they were, they would require ages much older than the distribution suggested by the HR diagram. We instead suggest

that these are in fact either extremely embedded cluster members or heavily extincted background field stars ($A_V > 20$ - 30). Either of these possibilities suggests that our derived IMF is in fact an upper limit to actual IMF below the hydrogen burning limit. Experiments studying the effects of extinction on the model KLF by Meageth (1996) and Comeron, Rieke & Rieke (1996) found that while extinction tended to shift the LFs to fainter magnitudes, the slope of the KLF was preserved. Thus, the steeply falling slope at the low mass end of the derived Trapezium IMF is reflective of the actual underlying IMF. However the true IMF may turnover at a larger mass than that implied by our present models. In the lower panel of Figure 11, the mass function derived from the Trapezium KLF is compared to that of Hillenbrand (1997) derived from spectroscopic observations. The two mass functions are generally very similar. In particular, these two mass functions agree very well at the high mass end ($M_\star > 2.0\ M_\odot$). For masses in the range $2.0\ M_\odot > M_\star > 0.5\ M_\odot$ the IMF derived from modeling the luminosity function contains more stars than that derived by Hillenbrand. However it is not clear how significant this difference is given the possible systematic uncertainties involved in both methods for determining the IMF and the fact that these two IMFs sample different volumes of the Orion Nebula region. For masses below $M_\star < 0.1\ M_\odot$, the IMF derived from the KLF modeling also contains considerably more stars than the spectroscopic IMF. However this difference is also not likely to be significant either since the spectroscopic IMF of Hillenbrand (1997) is not complete below $0.1\ M_\odot$.

Lastly, we can investigate whether the field star IMF (FSIMF) could also produce a KLF which reasonably matched the Trapezium KLF. To test this, we used the recent field star IMF parameterization from Scalo (1998). Scalo (1998) suggested a multiple power law IMF with the form:

$$\Gamma = \begin{cases} -0.20 & : \quad 1.0\ M_\odot > M_\star > 0.1\ M_\odot \\ -1.70 & : \quad 10.\ M_\odot > M_\star > 1.0\ M_\odot \\ -1.30 & : \quad M_\star > 10.\ M_\odot \end{cases} \tag{5}$$

Comparing the IMF in equation 4 to the field star IMF in equation 5, one finds that these two IMFs are quite similar, although for stars in the range of $10.0 > M/M_\odot > 1.0$, the Scalo IMF is steeper than the IMF in equation 4. In addition the Scalo IMF does not extend below the hydrogen burning limit. To facilitate comparison to the Trapezium data, we added a fourth power-law to the Scalo IMF to account for the faintest stars. We varied m_{break}, the mass at which the fourth power-law begins, between 0.06 and 0.1 $M_\odot$. In addition, we varied the slope of the fourth power-law (between -1.0 and +2.0). The best fits are also listed in Table 2. Using this modified field star IMF did yield a $\chi^2 \sim 1$ with an IMF that breaks near the hydrogen burning limit and falls with a similar steep slope as in the prior IMF fits.

To the extent that our adopted KLF represents the true KLF of the cluster, our modeling suggests that the IMF for brown dwarfs in the Trapezium cluster falls relatively steeply with decreasing mass. However because contamination due to reddened background stars and incompleteness due to nebular confusion has not properly been taken into account in the construction of the Trapezium KLF, the form of the derived IMF below the hydrogen burning limit should be regarded with

appropriate caution. As shown in Lada & Lada (1995) and Lada (Alves), one can use control-field observations (which are not available for this dataset) to gauge the completeness and membership at the faint end of the LF. Also, our present modeling has not included the effects of extinction and infrared excess. Hillenbrand et al., (1998), using the (I-K) diagnostic, found an average K band excess of 0.35 among identified optically visible cluster members. This average excess is smaller then the bins we have used to construct the Trapezium KLF, and therefore should have only a minor effect. Yet we can improve the derived IMF for the Trapezium cluster by constraining these effects using multi-wavelength observations and infrared color-color diagrams of the cluster and of near-by control fields. In a subsequent paper, we will use new JHK near-infrared observations and appropriate control fields to accurately determine the completeness of the Trapezium KLF and model the effects of extinction and infrared excess on the cluster KLF and the derived IMF.

Overall, we conclude from our modeling that the IMF of the Trapezium cluster is well represented by a three power-law mass function with a high mass slope between -1.00 and -1.7, a break in slope between 1 and 0.6 $M_\odot$ followed by a relatively flat or slightly rising slope to the hydrogen burning limit and then falling with a steep slope $\sim +1$ through the brown dwarf regime.

5. Conclusions

We have performed a series of experiments aimed at studying how the pre-main-sequence mass-to-luminosity relation, star forming history and initial mass function each affect the form of the luminosity function for populations of young pre-main sequence stars. Using models of the near-infrared luminosity function and varying these primary inputs, we have derived the following simple conclusions about model near-infrared luminosity functions:

- We find that the KLF of a young cluster is considerably more sensitive to variations in its underlying IMF than to either variations in the star forming history or the PMS mass-to-luminosity relation.
- PMS luminosity functions evolve in a systematic manner with increasing mean age and age spread. They evolve to fainter magnitudes and widen systematically with age.
- The KLFs of young stellar populations are found to be generally insensitive to variations in the adopted PMS mass-to-luminosity relations. In the youngest, coeval clusters, the presence of deuterium burning can produce significant features in the KLF which are sensitive to the adopted mass to luminosity relation. However even a small departure from a purely coeval star forming history will render these features difficult to detect observationally.

We model the observed luminosity function of the Trapezium Cluster and are able to derive an underlying IMF for the cluster which spans a range of stellar mass from 5 $M_\odot$ to 0.02 $M_\odot$, well into the brown dwarf regime. The IMF we derive is the simplest multiple power-law function which

can reproduce the observed luminosity function of the cluster given the mean age and star forming history derived from previous optical spectroscopic studies (Hillenbrand 1997). The derived IMF for the Trapezium cluster consists of three power law segments, has a peak near the hydrogen burning limit and steadily decreases below the hydrogen burning limit and throughout the brown dwarf regime. We derive a brown dwarf mass spectrum of the form dN/dlogm $\sim\ m^{+1}$ ($0.08 > M/M_{\odot} > 0.02$). However, the form of the IMF below the hydrogen burning limit must be regarded with caution since the faint end of the observed cluster KLF has not been adjusted for the possible effects of background star and nebular contamination. Above the hydrogen burning limit, the Trapezium IMF is also consistent with that recently advocated for field stars by Scalo (1998).

We thank Richard Elston for conversations and suggestions on the use of Monte Carlo techniques. We also thank João Alves, Alyssa Goodman, Pavel Kroupa, John Scalo and John Stauffer for conversations and suggestions which improved upon this work. A.A.M. is supported by a Smithsonian Predoctoral Fellowship. EAL acknowledges support from a Research Coorporation Innovation Award, a NSF PECASE Grant, AST-9733367, and a NASA ADP grant NAG5-6751 to the University of Florida, Gainesville.

A. Bolometric Corrections

Bolometric corrections were interpolated from a table of basic stellar properties to convert model stars' luminosities and effective temperatures into monochromatic magnitudes. The following formulae were used to convert from these theoretical quantities to the monochromatic pass band magnitude.

$$\mathrm{M}_{\lambda} = \mathrm{M}_{bol,\star} - \mathrm{BC}_{\lambda} \quad \text{(A1)}$$

$$\mathrm{M}_{bol,\star} = \mathrm{M}_{bol,\odot} - 2.5 * \log(L/L_{\odot}) \quad \text{(A2)}$$

$$\mathrm{M}_{\lambda} = \mathrm{M}_{bol,\odot} - 2.5 * \log(L/L_{\odot}) - \mathrm{BC}_{\lambda} \quad \text{(A3)}$$

We have adopted the near-infrared colors of dwarf stars. While the temperature scales for young pre-main sequence stars fall somewhere between the temperature scales for main sequence dwarfs and giants (Luhman 1999), their near-infrared colors are more dwarf-like (Luhman 1999).

We constructed our table of stellar properties beginning with those compiled in Kenyon & Hartmann (1995) (KH95). We adjusted this tabulation to reflect the large temperature range of our model stars and to investigate some of the dependencies of our models on this tabulation. For spectral types O3 to B0.5, corresponding to T_{eff} from 30,000 to 50,000 K, we used V band bolometric corrections and effective temperatures from Vacca et al., (1996). O star colors were assumed degenerate at all near-infrared bands and assigned the colors of Johnson (1966). B star red and near-infrared colors were taken from a recent tabulation by Winkler (1997). There is presently a significant study in the literature of the color-T_{eff}-spectral type relation for cool stars with T_{eff}

less than 3500K (Leggett et al., 1996). Because we related the stellar effective temperature directly to the stellar color and bolometric correction and do not assign spectral types to our model stars, we do not need to define any particular spectral sequence. For the color-T_{eff}-BC_V relation of M dwarfs, we used the relations compiled by Bessell et al. (1991,1995,1998). However, our model stars have effective temperatures much cooler than those defined by the observationally defined scales. To extend our color relations to even cooler effective temperatures, we used the broad band fluxes from model atmosphere and PMS evolutionary calculations by Baraffe et al., (1998). Though typical model atmosphere calculations have been used to fit spectra and develop spectral sequences for sometime, the predicted broadband fluxes from these model atmospheres have been largely inaccurate (Leggett 1992; Graham et al., 1992; Kirkpatrick et al., 1993a; Tinney, Mould & Reid 1993; Leggett et al., 1996). Baraffe et al., (1998) models are the most recent calculations of both synthetic spectra and broadband fluxes for cool stars and brown dwarfs and employ the most recent opacity tables. After examining their different calculations and predicted cool stars colors, we used their 10 Gyr models to extend our color-T_{eff}-BC_V tabulation at all red and near-infrared bands.

We checked our tabulation against other recent compilations of stellar properties and cool stars observations in the literature. We compared our T_{eff}-BC_V relation to those polynomial fits recently derived by Flower (1996) and Hillenbrand (1997). We found that our tabulation was in systematic disagreement with these fits. The cause was traced to the original Schmidt-Kaler (1982) T_{eff}-BC_V tabulation used in the KH95 compilation. We refer to the discussion in Bessell, Castelli & Plez (1998) (their Appendix D) as to the source of this discrepancy and follow their prescription to add +0.12 to the Schmidt-Kaler (1982) BC_V scale. Combined with our choice of $M_{bol,\odot}$ equal to 4.75, this yielded a solar BC_V equal to -0.07 and an absolute $M_{V,\odot}$ magnitude of 4.81. We then smoothed the T_{eff}-BC_V relation to match those of Hillenbrand (1997) and Flower (1996).

A more important concern is the accuracy of our tabulation below 3500K. We tested our tabulation for cool stars by compiling, from the literature, observed colors, effective temperature determinations and bolometric luminosities for M dwarfs from the literature including published data by Berriman, Reid & Legget (1992), Tinney, Mould & Reid (1993), Jones et al., (1994) and Leggett et al., (1996). We used repeat observations and derivations of stellar properties (e.g. T_{eff}) of the same M dwarfs but by different authors as reflecting different spectral type to effective temperature scales and variability among late-type stars, as well as fundamental uncertainties in the computation of these values. The observed M dwarf colors, bolometric corrections, and effective temperatures were compared to our compiled table. First, our comparison indicated that the compiled bolometric corrections were consistent with the observed M dwarf values. Second, and more importantly, our comparison showed that for the near-infrared bands, specifically the K band, the bolometric corrections are insensitive to effective temperature scales for low mass stars and brown dwarfs.

B. Combining Pre-Main Sequence Tracks

A set of theoretical evolutionary sequences were used to convert the masses and ages of model stars to luminosities and effective temperatures which were then converted to monochromatic pass-band magnitudes using the color tabulation documented in Appendix A. These sequences were a combination of three different regimes: a theoretical zero age main sequence, a set of intermediate mass PMS tracks and a set of sub-solar and brown dwarf PMS stellar models. When converting the model stars, the algorithm determined if, for certain stellar age, the star would be found on the ZAMS or in a PMS stage. If the star would be found on the ZAMS, then it luminosity and effective temperature was derived from the ZAMS. If the star would be in a PMS stage, then the PMS models were used.

Unfortunately, PMS theoretical models are not typically calculated for the entire mass range from brown dwarfs to high mass B stars. Because of this, we combined two different sets of PMS tracks to provide a complete mass range. We took the opportunity to use different sets of PMS tracks for high and low mass stars to account for an apparent mass-age correlation found by many authors who have used PMS tracks to derive real ages and masses for stars using the HR diagram (Hillenbrand 1994; Meyer 1996; Hillenbrand 1997). These authors point out that when masses and ages are derived for a cluster of real stars using PMS models, a correlation existed such that the more massive stars were systematically older than lower mass stars. These authors suggested that the cause of this correlation is due to the way canonical PMS tracks are constructed. Canonical PMS tracks evolve the model stars from infinite spheroids. More recent studies suggest that stars evolve during a protostellar phase along a specific mass-radius relationship referred to as the proto-stellar birthline (Stahler 1983; Palla & Stahler 1993). Using a proto-stellar birthline as the initial condition for PMS tracks will most prominently affect the predicted luminosities and effective temperatures of the youngest and highest mass stars, where the stars' proto-stellar (birthline) lifetimes are comparable with these stars' pre-main sequence lifetimes.

Rather than using canonical PMS tracks for model stars with masses greater than solar, we used "accretion scenario" PMS model calculations by Palla & Stahler (1993) and Bernasconi (1996a). Accretion scenario PMS models better represent the location of the young intermediate mass stars on the HR diagrams (Palla & Stahler 1993; Bernasconi & Maeder 1996b). Yet the accretion scenario PMS tracks cannot be straightforwardly used with sub-solar mass canonical PMS tracks. We adopted the accretion scenario tracks for models above 2 solar masses and canonical tracks below 1 solar mass. Between these two limits, we compared the canonical and accretion scenario calculations. We performed an average of the accretion scenario and canonical mass tracks, weighting each average to result in a smooth conversion from the canonical (sub-solar mass) to accretion scenario (high) regimes. We examined the theoretical HR diagram resulting from our combination of ZAMS, accretion scenario, averaged, and canonical PMS tracks. This new set of tracks and resulting isochrones were found to be smooth between all regimes and was used as input for the luminosity function modeling.

REFERENCES

Alexander, D. R., Augason, G. C., & Johnson, H. R. 1989, ApJ, 345, 1014

Alexander, D. R., & Ferguson, 1994, ApJ, 437, 879

Ali, B., & DePoy, D. L., 1995, AJ, 109, 709

Baraffe, I., Chabrier, G., Allard, F., & Hauschildt, P. H. 1998, A&A, 337, 403

Belikov, A. N. & Piskunov, A. E. 1997, ARep, v. 41, no. 1, 28

Belikov, A. N., Hirte, S., Meusinger, H., Piskunov, A. E., & Schilbach, E. 1997, A&A, 332, 575

Bernasconi, P. A. 1996, A&AS, 120, 57

Bernasconi, P. A., & Maeder, A. 1996, A&A, 307, 829

Berriman, G. B., Reid, I. N., & Leggett, S. K. 1992, ApJ, 392, L31

Bessell, M. S. 1991, AJ, 101, 662

Bessell, M. S. 1995, Proceedings of the ESO Workshop: The Bottom of the Main Sequence - and Beyond, ed C. G. Tinney, (Heidelberg: Springer), 123

Bessell, M. S., Castelli, F., & Plez, B. 1998, A&A, 333, 231

Canuto, V. M., & Mazzitelli, I. 1990, ApJ, 370, 295

Canuto, V. M., & Mazzitelli, I. 19 92, ApJ, 389, 724

Canuto, V. M., Goldman, I., & Mazzitelli, I. 1996, ApJ, 473, 550

Comeron, F., Rieke, G. H., & Rieke, M. J. 1996, ApJ, 473, 294

D'Antona, F. & Mazzitelli, I. 1983, A&A, 127, 149

D'Antona, F. & Mazzitelli, I. 1994, ApJS, 41, 467

D'Antona, F. & Mazzitelli, I. 1998, Cool Stars in Clusters and Associations, ed G. Micela and R. Pallavicini, (Mem. S.A.It.), 68, 807

Fletcher, A. B., & Stahler, S. W. 1994, ApJ, 435, 313

Fletcher, A. B., & Stahler, S. W. 1994, ApJ, 435, 329

Flower, P. 1996, ApJ, 469, 355

Graham, J. R., Matthews, K., Greenstein, J. L., Neugebauer, G., Tinney, C. G., and Persson, S. E. 1992, AJ, 104, 2016

Herbig, G. H. 1998, ApJ, 497, 736

Hillenbrand, L. A. 1994, Ph.D thesis UMass. Amherst

Hillenbrand, L. A. 1997, AJ, 114, 198

Hillenbrand, L. A., & Hartmann, L. W. 1998, ApJ, 492, 540

Hillenbrand, L. A., Strom, S. E., Calvet, N., Merrill, K. M., Gatley, I., Makidon, R., Meyer, M. R., & Skrutskie, M.F. 1998b, AJ, 116, 1816

Ibsen, I. 1965, ApJ, 141, 993

Johnson, H. L. 1966, ARA&A, 4, 193

Jones, H. R. A., Longmore, A. J., Jameson, R. F., & Mountain, C. M. 1994, MNRAS, 267,413

Kenyon, S. J., & Hartmann, L. W. 1995, ApJS, 101, 117

Kirkpatrick, J. D., Kelly, D. M., Rieke, G. H., Allard F., & Wehrse, R. 1993, ApJ, 402, 643

Kroupa, P., Tout, C. A., & Gilmore, G. 1993, MNRAS, 262, 545

Kurucz, R. L. 1991, in Stellar Atmospheres: Beyond the Classical Models, ed L. Crivellari, I. Hubeny, & D. G. Hummer, (Dordrecht: Kluwer), 441S

Lada, C. J., Alves J., and Lada, E. A. 1996, AJ, 111, 1964

Lada, E. A., Lada, C. J., & Muench, A. A. 1998, 38th Herstmonceux Conference: The Stellar Initial Mass Function, Gerry Gilmore and Debbie Howell, San Francisco: A.S.P, 107

Lada, E. A., & Lada, C. J. 1995, AJ, 109, 1682

Lada, E. A. 1999, in The Origin of Stars and Planetary Systems, ed C. J. Lada & N. D. Kylafis, (Dordrecht: Kluwer), p. 441

Leggett, S. K. 1992, ApJS, 82, 351

Leggett, S. K., Allard, F., Berriman, G. B., Dahn, C. C., & Hauschildt, P. H. 1996, ApJS, 104, 117

Luhman, K. L. 1999, ApJ, 525, 466

Mazzitelli, I. 1972, Ap&SS, 17, 378

McCaughrean, M., Zinnecker, H., Rayner, J., and Stauffer, J. 1995, Proceedings of the ESO Workshop: The Bottom of the Main Sequence - and Beyond, C. G. Tinney, Springer: Heidelberg, 207

Meageth, S. T. 1996, A&A, 311, 135

Meyer, M. R. 1996, Ph.D thesis UMass. Amherst

Miller, G. E., & Scalo, J. M. 1979, ApJS, 41, 513

Palla, F., & Stahler, S. W. 1993, ApJ, 418, 414

Salpeter, E. E. 1955, ApJ, 121, 161

Scalo, J. 1998, 38th Herstmonceux Conference: The Stellar Initial Mass Function, ed Gerry Gilmore and Debbie Howell, (San Francisco: A.S.P), 201

Schaller, G., Schaerer, D., Meynet, G., & Maeder, A 1992, A&AS, 96, 269

Schmidt-Kaler, T. 1982, Landolt-Börnstein, Group VI. Vol. 2, ed K.-H. Hellwege, (Berlin: Springer), 454

Stahler, S. W. 1983, ApJ, 274, 822

Strom, K. H., Strom, S. E., & Merrill, K. 1993, ApJ, 412, 233

Tinney, C. G., Mould, J. R., & Reid, I. N. 1993, AJ, 105, 1045

Vacca, W. D., Garmany, C. D., & Schull, J. M. 1996, ApJ, 460, 914

Winkler, H. 1997, MNRAS, 287, 481

Zinnecker, H., McCaughrean, M., & Wilkings, B. A. 1993, Protostars and Planets III, ed H. Levy and J. I. Lunine, (Tucson: Univer. of Arizona), 429

Fig. 1.— Definitions of age and age spread used to define the cluster star forming history in modeling the cluster KLF throughout this paper. The mean age, τ, in this simple model is equivalent to the average of the ages of the oldest and youngest stars assuming a constant rate of star formation throughout the star forming history of the cluster.

Fig. 2.— Model KLFs derived from the four sets of PMS models of DM94. Each corresponds to a different combination of input physics as described in DM94 (see also Table 1). These model KLFs used a log-normal IMF with a lower mass limit of 0.1 $M_{\odot}$ and coeval star formation with mean ages of 1 (top) and 7 (bottom) Myrs. Different symbols correspond to different input opacity tables in the PMS models used. The number of stars in each bin corresponds to the mean value of that bin for 100 independent realizations of the model KLF. Each realization of the model KLF contains 1000 stars. Error bars are 1 σ standard deviation of the mean value of that bin for the 100 iterations of the model.

Fig. 3.— Model KLFs comparing the input PMS models from DM94 and DM98. Shown are model KLFs computed using the ACM model of DM94 and the d2.5 model from DM98 (see Table 1). These two PMS evolutionary models differ in basic input physics such as opacity table, equation of state and treatment of convection. However they have identical mass ranges and deuterium abundances. Both panels correspond to model KLFs for clusters with a coeval star forming history and mean ages of 0.8 Myrs (top panel) and 5 Myrs (bottom panel). Error bars are the same as those in Figure 2.

Fig. 4.— Model KLFs derived from DM98 PMS models varying the fractional deuterium abundance at the onset of pre-main sequence contraction. These model KLFs have the standard log-normal IMF sampled over the complete mass range available for the DM98 PMS models (see Table 1). The first column of panels are for coeval SFHs with mean ages of 2 and 7 Myrs. In the second column of panels, we display model KLFs with the same mean ages but with age spreads that are twice the value of the mean age. The different model KLFs are labeled corresponding to the deuterium abundance ratio relative to hydrogen and given in units of $\times 10^{-5}$. Physically, these abundances represent one half, one and two times the measured interstellar medium abundance of deuterium. Error bars are the same as those in Figure 2.

Fig. 5.— Model KLFs testing the inclusion into model KLFs of high and intermediate mass stars as well as stars at the hydrogen burning limit and brown dwarfs. The mass to luminosity relation was extracted from the ACM PMS model of DM94, intermediate mass PMS tracks of Palla & Stahler (1993) and a ZAMS from Schaller et al., (1992) for higher mass stars. Two different mean ages and SFH histories are shown for illustration. In the upper panel, model KLFs created using a coeval star forming history and a mean age of 3.0 Myrs. The lower panel shows a model KLF with a continuous star forming history over the lifetime of the cluster and a mean age of 5 Myrs. Error bars are the same as those in Figure 2.

Fig. 6.— Model KLFs varying the cluster mean age and age spread. Each panel displays a different

$\Delta\tau/\tau$. Mean ages shown are 1, 3 and 10 million years. Note that from panel to panel, features in the model KLF caused by inflections in the M-L relation are smoothed by increased age spread. The apparent break in the model KLFs in the last bin of each KLF is primarily due to incompleteness in that bin due to a truncation of the M-L relation at 0.02 $M/M_{\odot}$. Please see section 3.3 for further explanation. Error bars are the same as those in Figure 2.

Fig. 7.— Plot illustrating the evolution of the KLF mean with increasing cluster age and age spread. The KLF mean refers to the arithmetic mean of the K magnitudes for all synthetic cluster members. Two sets of values are plotted for KLFs having two different underlying IMFs. "With Brown Dwarfs" contains stars below 0.1 $M_{\odot}$ and "Without Brown Dwarfs" has no stars less than 0.1 $M_{\odot}$. For each set of curves, the KLF mean was plotted for the two extremes of possible star forming histories. Error bars are not shown but are within the size of the plotting symbols for a cluster of 1000 stars.

Fig. 8.— Model KLFs plotted to show the effects of varying the cluster age spread. Synthetic cluster KLFs with mean ages of $\tau = 1$ and 6 Myrs, respectively, are shown in each panel. For each mean age (in each panel) the same four age spreads from Figure 6 are over-plotted. Increasing age spread erases features in the KLF caused by inflections in the mass to luminosity relation. Error bars are the same as those in Figure 2.

Fig. 9.— Different mass functions used in modeling experiments. A few different parameterizations are shown. The log-normal form follows the parameterization of MS79 and is extended to the mass limit, 0.02 $M_{\odot}$, of our model KLFs. The other IMFs shown are examples of the simple 2 power law IMFs used for experiments in section 3.3. The high mass IMF slope, Γ_1, equals -1.35 equivalent to the power law IMF derived by Salpeter (1955). This power-law breaks at a mass, m_{break}, equal to 0.5 $M_{\odot}$. Below the break mass, the IMF is governed by a low mass slope, Γ_2, for which we show five different values, -1.35, -1.00, -0.40, 0.00, +0.40, and +1.0.

Fig. 10.— KLF models using the 2 power law IMF described in equation 3. The different model KLFs are normalized to have identical bright slope LFs where their underlying IMFs are identical. The left panel shows the resulting KLFs corresponding to the underlying IMFs shown in the right hand panel. Symbols are identical for underlying IMFs and the resulting model KLF.

Fig. 11.— Top panel: The histogram is the combined KLF for the Trapezium from Zinnecker et al., (1993) and McCaughrean et al., (1995) KLFs. The model KLF is shown fit to the Trapezium KLF and uses the model (g) IMF from Table 2. Also shown is a model cluster KLF created using the Salpeter (1955) field star IMF extended to the mass limit (0.02 $M_{\odot}$). The model SFH is characterized by a constant star formation rate, a mean age of 0.8 Myrs (Hillenbrand 1997) and an age spread of 1.2 Myrs. Lower panel: Histogram of the Orion Nebula Cluster (ONC) IMF derived by Hillenbrand (1997) compared to model IMF (g) used for the fit model KLF in the upper panel. Also shown are the Salpeter (1955) field star IMF and the completeness limit in mass quoted by Hillenbrand (1997,1998). For comparison, model IMF (g) is scaled to contain the same number of

stars as the ONC IMF above its completeness limit. Error bars for the Hillenbrand IMF reflect one sigma counting statistics. The model KLF error bars are one sigma standard deviations as described in Figure 2.

Table 1. Pre-main Sequence Models Used

Model Name	Opacity Table	Convection Model	$[D/H]^a$	Mass Range ($M/M_\odot$)
		D'Antona & Mazzitelli (1994)		
ACM	Alexander et al. (1989)	FST[1]	2.0	0.018 → 2.5
AMT	Alexander et al. (1989)	MLT[2]	2.0	0.1 → 2.5
KCM	Kurucz (1991)	FST[1]	2.0	0.1 → 2.5
KMT	Kurucz (1991)	MLT[3]	2.0	0.1 → 2.5
		D'Antona & Mazzitelli (1998)[b]		
d1.5	Alexander & Ferguson (1994)	FST[4]	1.0	0.017 → 1.5
d2.5	Alexander & Ferguson (1994)	FST[4]	2.0	0.017 → 3.0
d4.5	Alexander & Ferguson (1994)	FST[4]	4.0	0.017 → 3.0

[a]Deuterium Abundance relative to Hydrogen; In units of $\times 10^{-5}$

[b]DM98 models were initially released in 1997. These models were updated in 1998. The model used were those of the updated calculations.

[1]Full Spectrum Turbulence Model; Canuto & Mazzitelli (1990, 1992)

[2]Mixing Length Theory; $1/H_p = 1.2$

[3]Mixing Length Theory; $1/H_p = 1.5$

[4]Full Spectrum Turbulence Model; Canuto et al., (1996)

Table 2. Model IMF Fits to Trapezium KLF

Name	χ^2 Prob.	Γ_0	m_{break}	Γ_1	m_{break}	Γ_2
Two Power Law Fits						
a	0.38	-	-	-0.50	0.10	+1.00
Three Power Law Fits						
b	0.71	-0.75	0.25	0.00	0.10	+0.75
c	0.86	-1.00	0.40	0.00	0.08	+1.00
d	0.88	-1.00	0.60	-0.25	0.10	+1.00
e	0.93	-0.75	0.25	-0.25	0.10	+0.75
f	0.99	-1.00	0.70	-0.25	0.08	+1.00
g	0.99	-1.35	0.80	-0.25	0.08	+1.35
Scalo 1998 Field Star IMF[1]+ BDIMF						
h	0.96	-1.70	1.00	-0.20	0.10	+0.75
i	0.99	-1.70	1.00	-0.20	0.08	+1.00

[1]Above 10 $M_\odot$, this IMF has a Γ equal to -1.30.

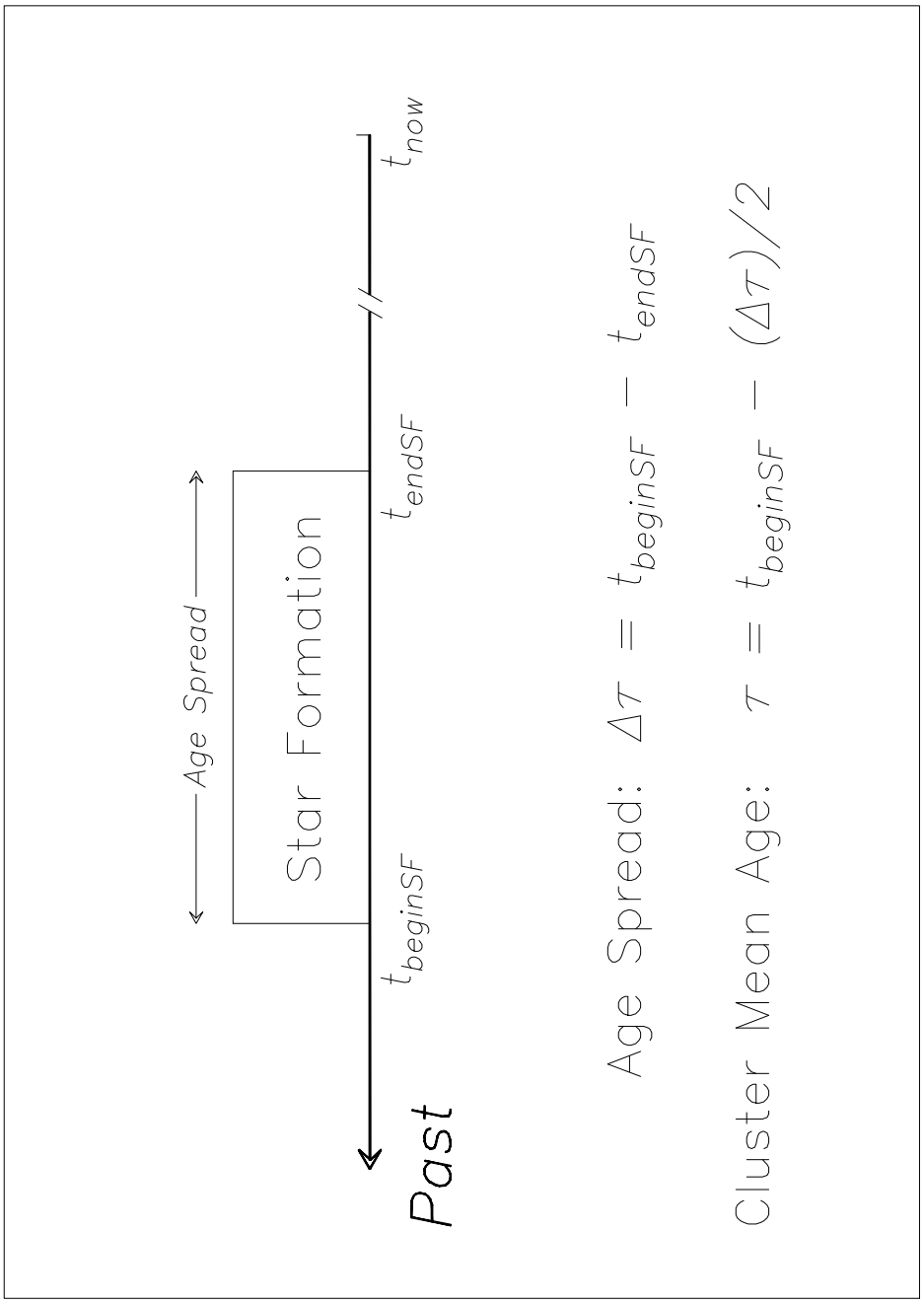
Cluster Dating Parameters
Age Spread
Star Formation
$t_{beginSF}$
t_{endSF}
t_{now}
Past
Age Spread: $\Delta\tau = t_{beginSF} - t_{endSF}$
Cluster Mean Age: $\tau = t_{beginSF} - (\Delta\tau)/2$

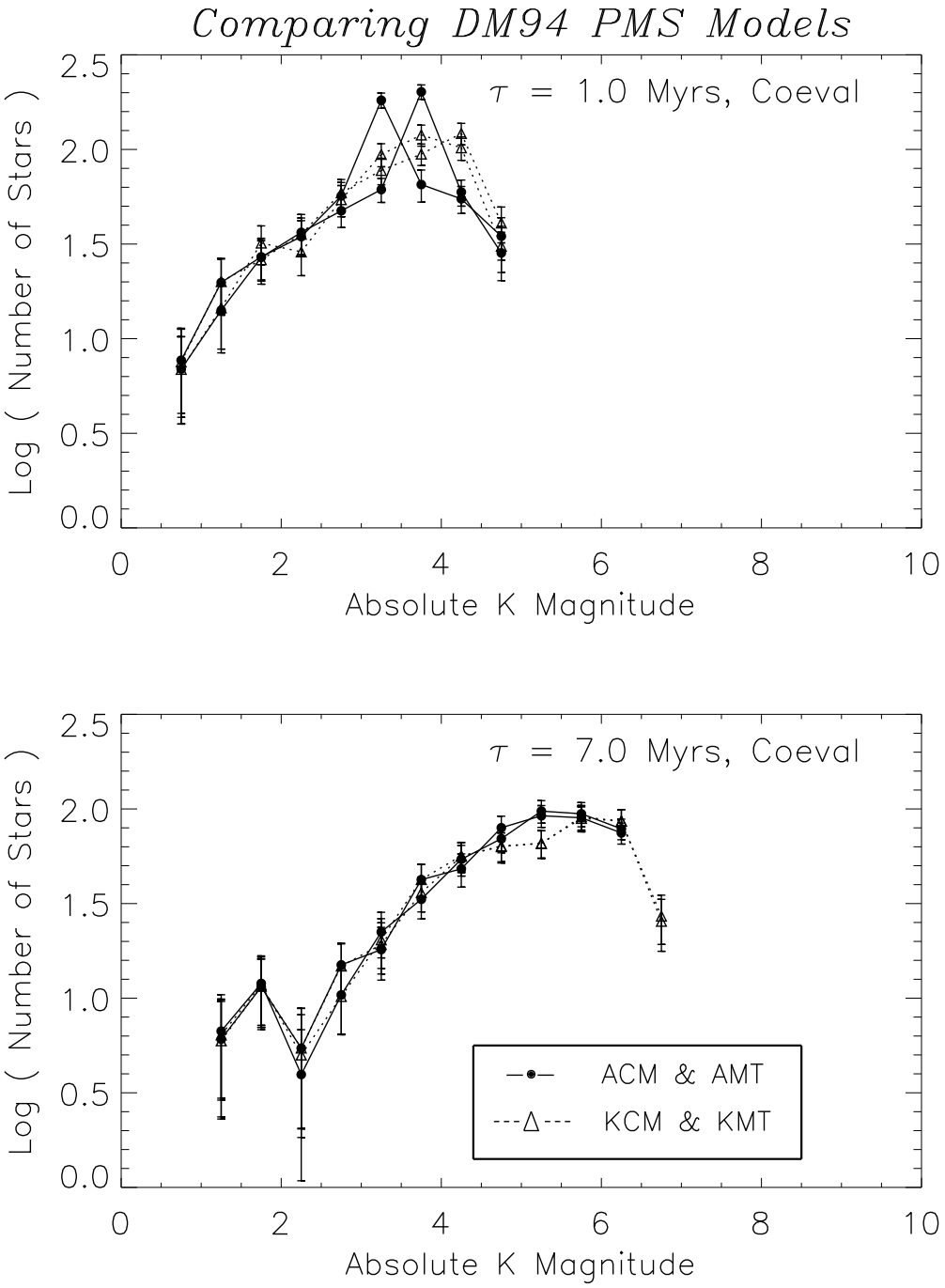
Comparing DM94 PMS Models
τ = 1.0 Myrs, Coeval
Log (Number of Stars)
Absolute K Magnitude
τ = 7.0 Myrs, Coeval
ACM & AMT
KCM & KMT
Log (Number of Stars)
Absolute K Magnitude

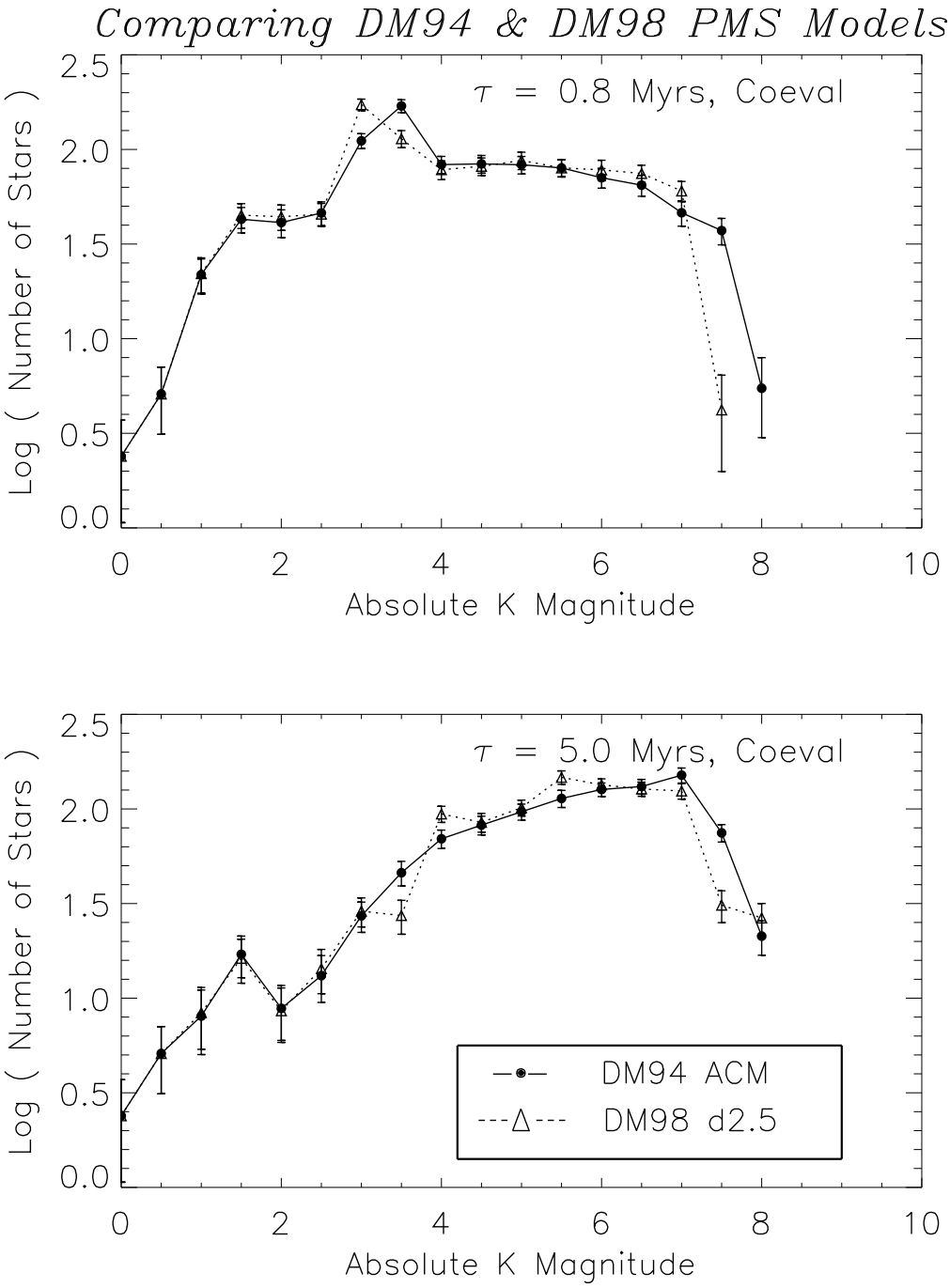
Comparing DM94 & DM98 PMS Models
τ = 0.8 Myrs, Coeval
τ = 5.0 Myrs, Coeval
Log (Number of Stars)
Absolute K Magnitude
DM94 ACM
DM98 d2.5

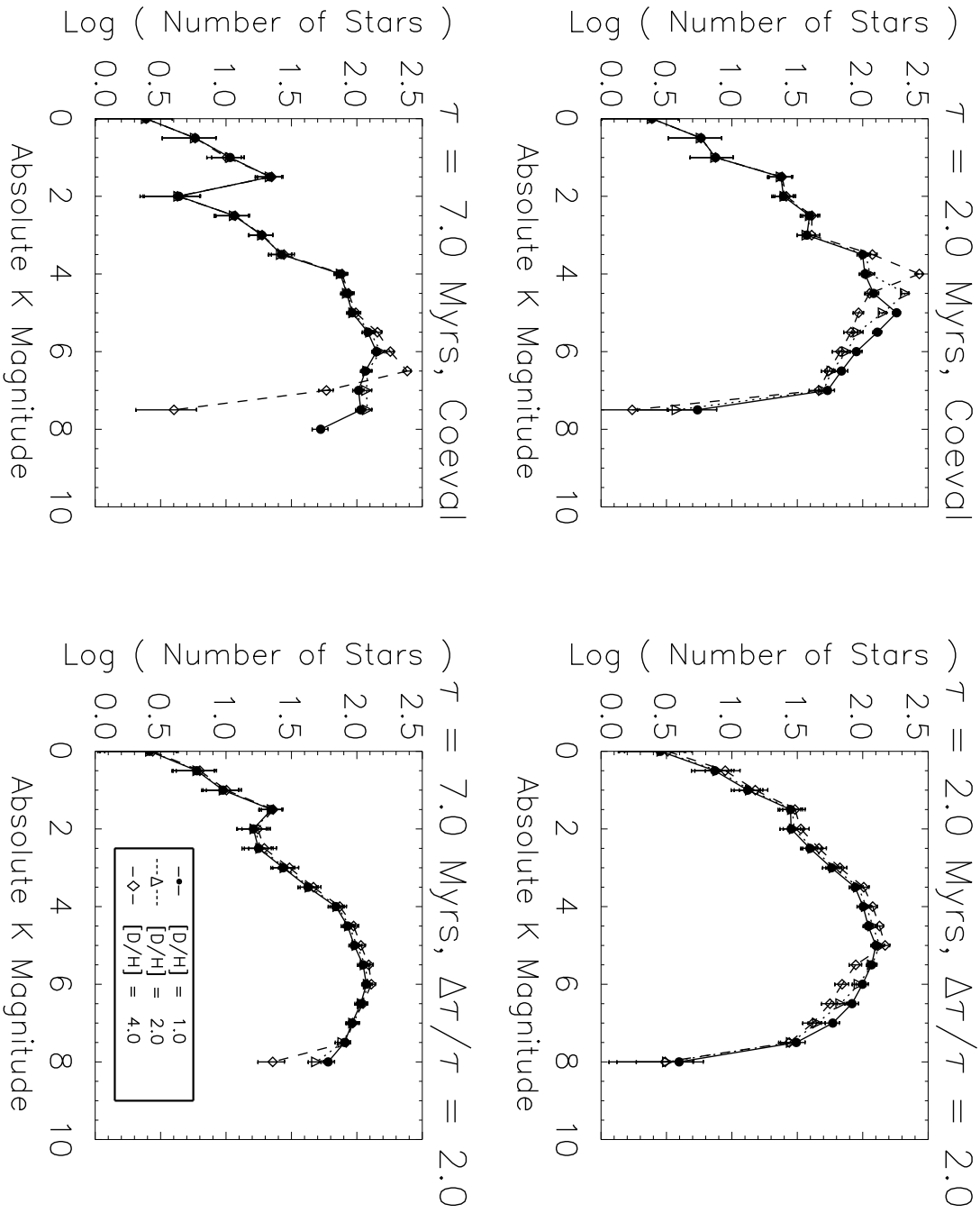
τ = 2.0 Myrs, Coeval
τ = 7.0 Myrs, Coeval
τ = 2.0 Myrs, Δτ/τ = 2.0
τ = 7.0 Myrs, Δτ/τ = 2.0
Log (Number of Stars)
Absolute K Magnitude
[D/H] = 1.0
[D/H] = 2.0
[D/H] = 4.0

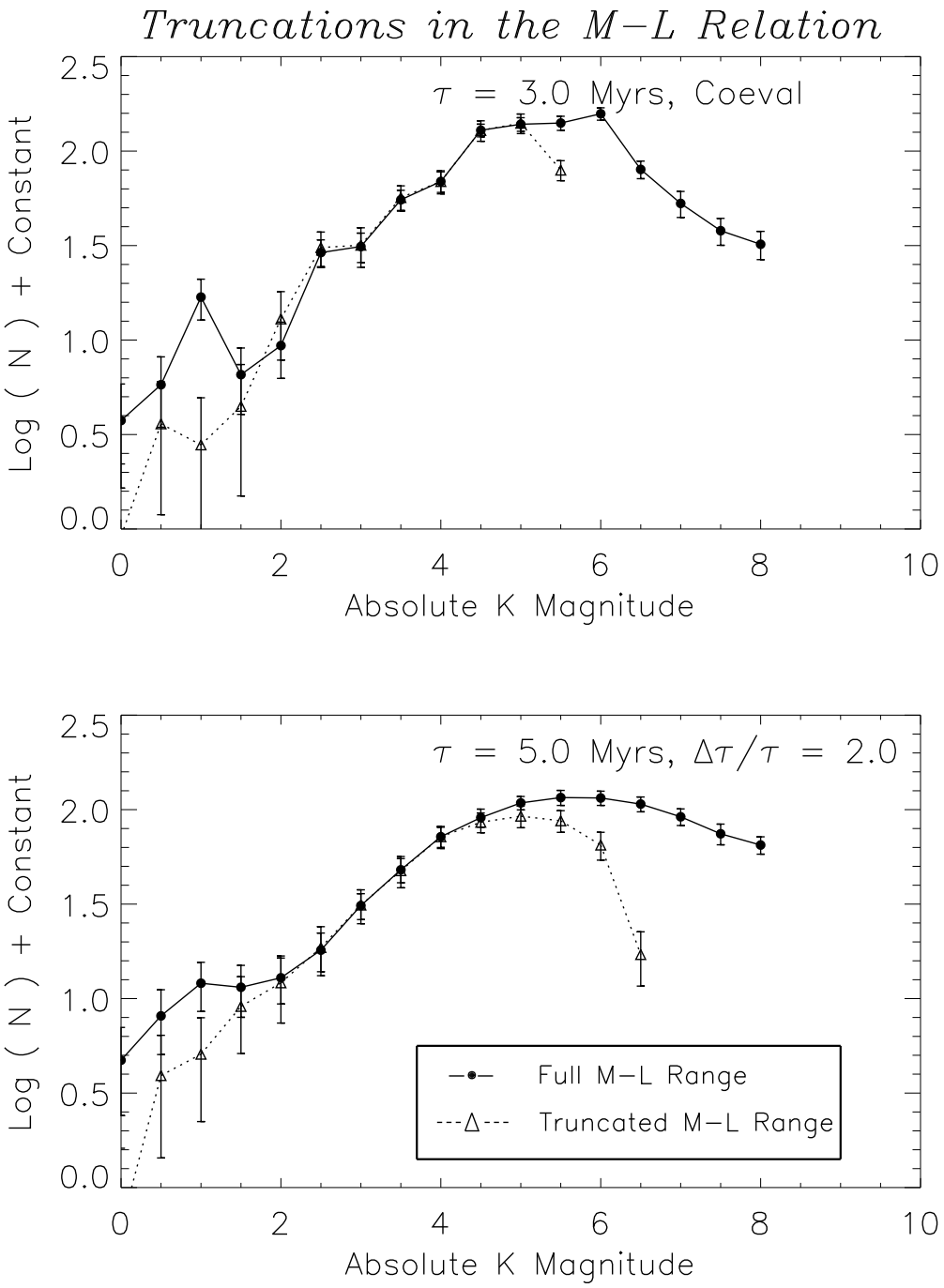
Truncations in the M−L Relation
τ = 3.0 Myrs, Coeval
Log (N) + Constant
Absolute K Magnitude
τ = 5.0 Myrs, Δτ/τ = 2.0
Full M−L Range
Truncated M−L Range
Log (N) + Constant
Absolute K Magnitude

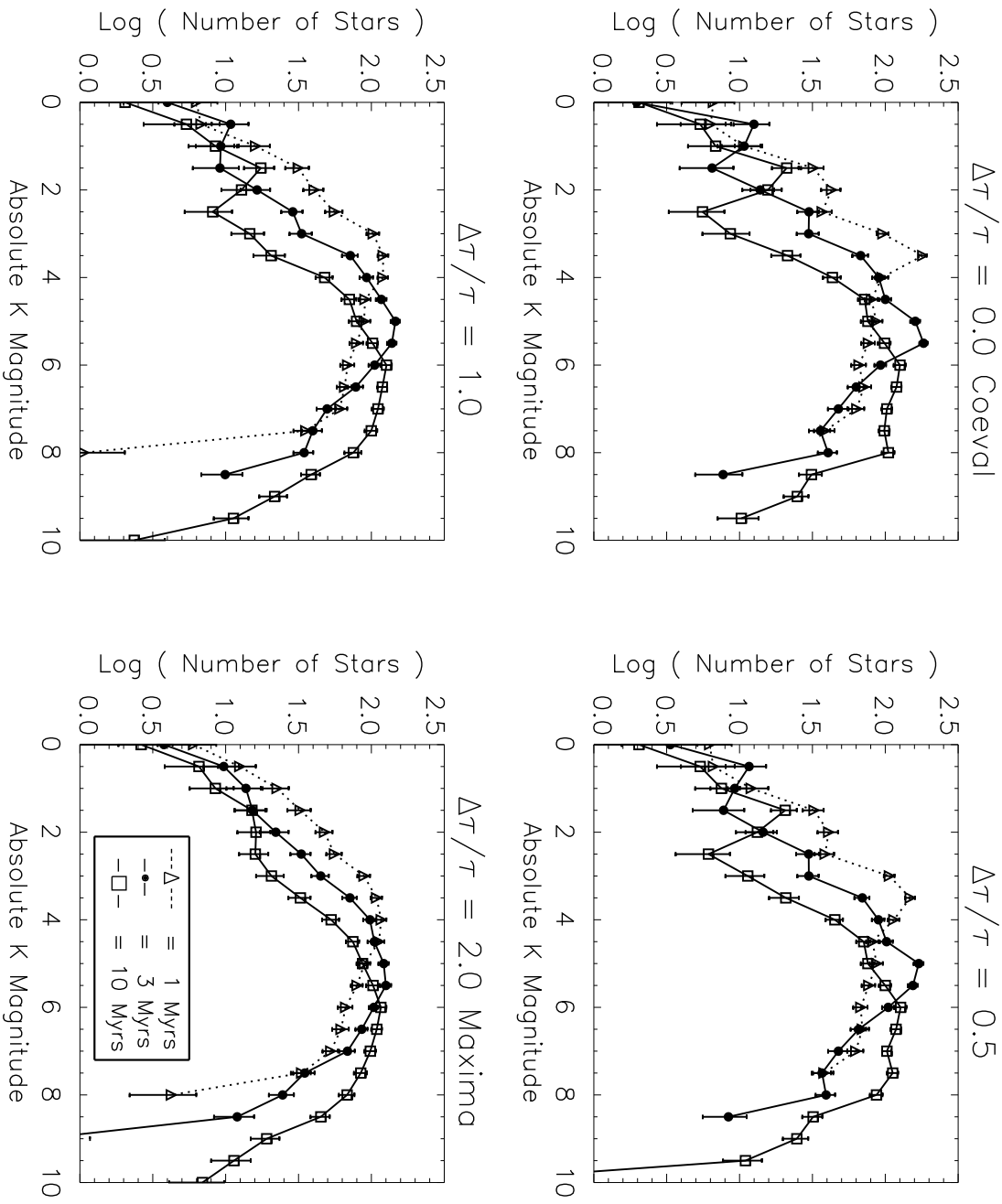
Log (Number of Stars)
Absolute K Magnitude
$\Delta\tau/\tau$ = 0.0 Coeval
$\Delta\tau/\tau$ = 0.5
$\Delta\tau/\tau$ = 1.0
$\Delta\tau/\tau$ = 2.0 Maxima
---Δ--- = 1 Myrs
—●— = 3 Myrs
—□— = 10 Myrs

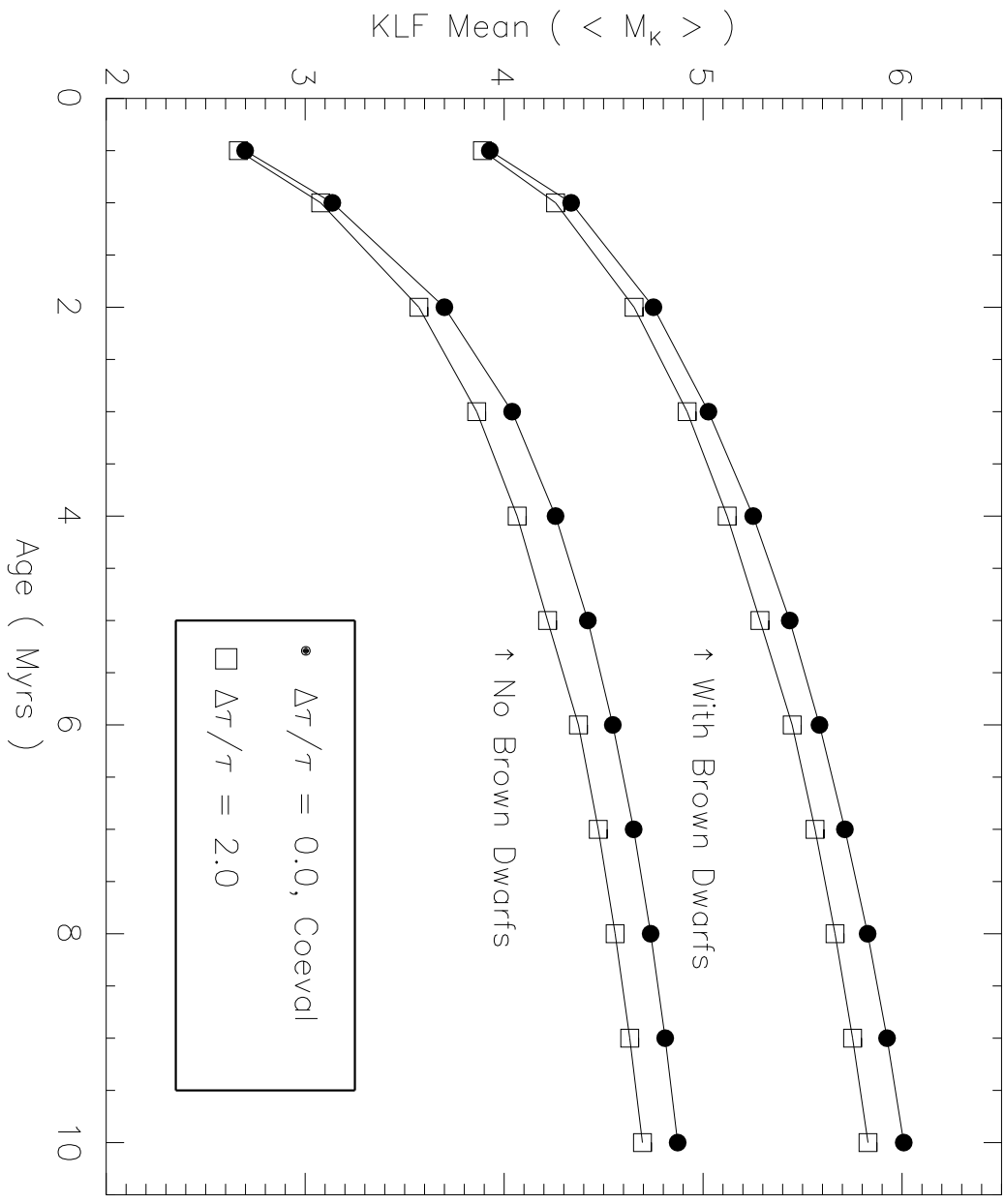
Mean K Magnitude Versus Mean Age
KLF Mean (< M_K >)
Age (Myrs)
2
3
4
5
6
0
2
4
6
8
10
With Brown Dwarfs
No Brown Dwarfs
$\Delta\tau/\tau$ = 0.0, Coeval
$\Delta\tau/\tau$ = 2.0

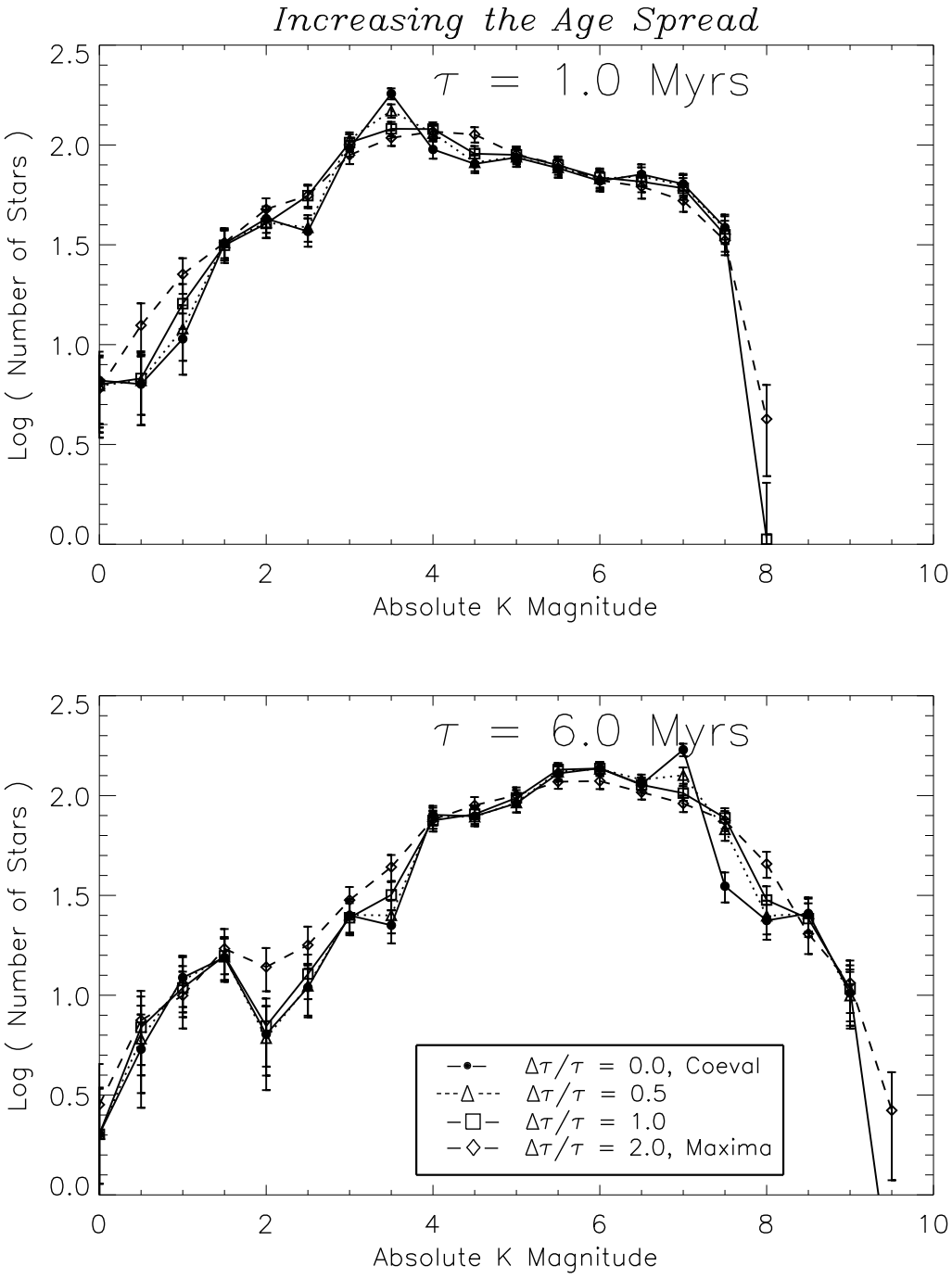
Increasing the Age Spread
τ = 1.0 Myrs
τ = 6.0 Myrs
Log (Number of Stars)
Absolute K Magnitude
Δτ/τ = 0.0, Coeval
Δτ/τ = 0.5
Δτ/τ = 1.0
Δτ/τ = 2.0, Maxima

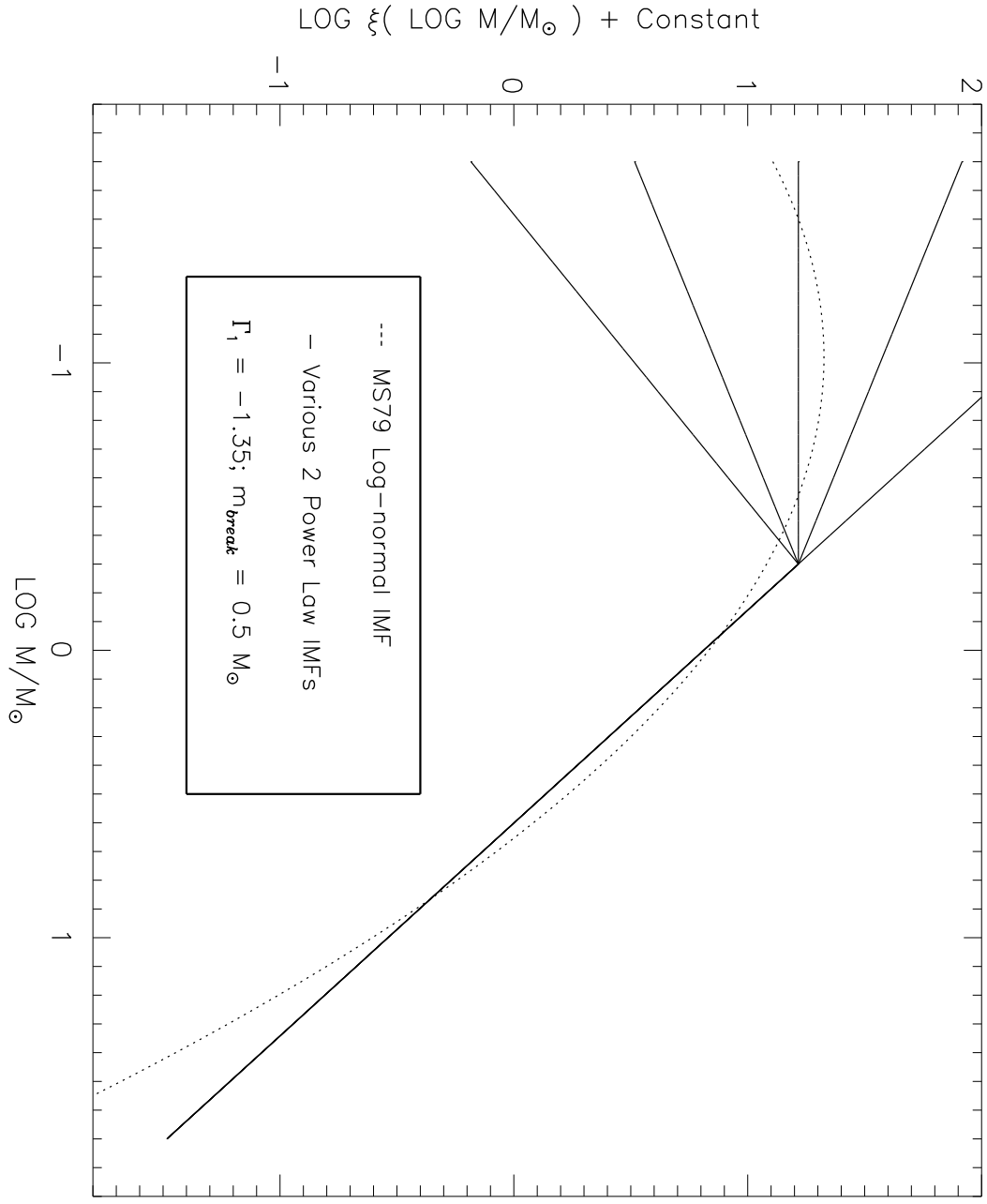

Initial Mass Functions Used

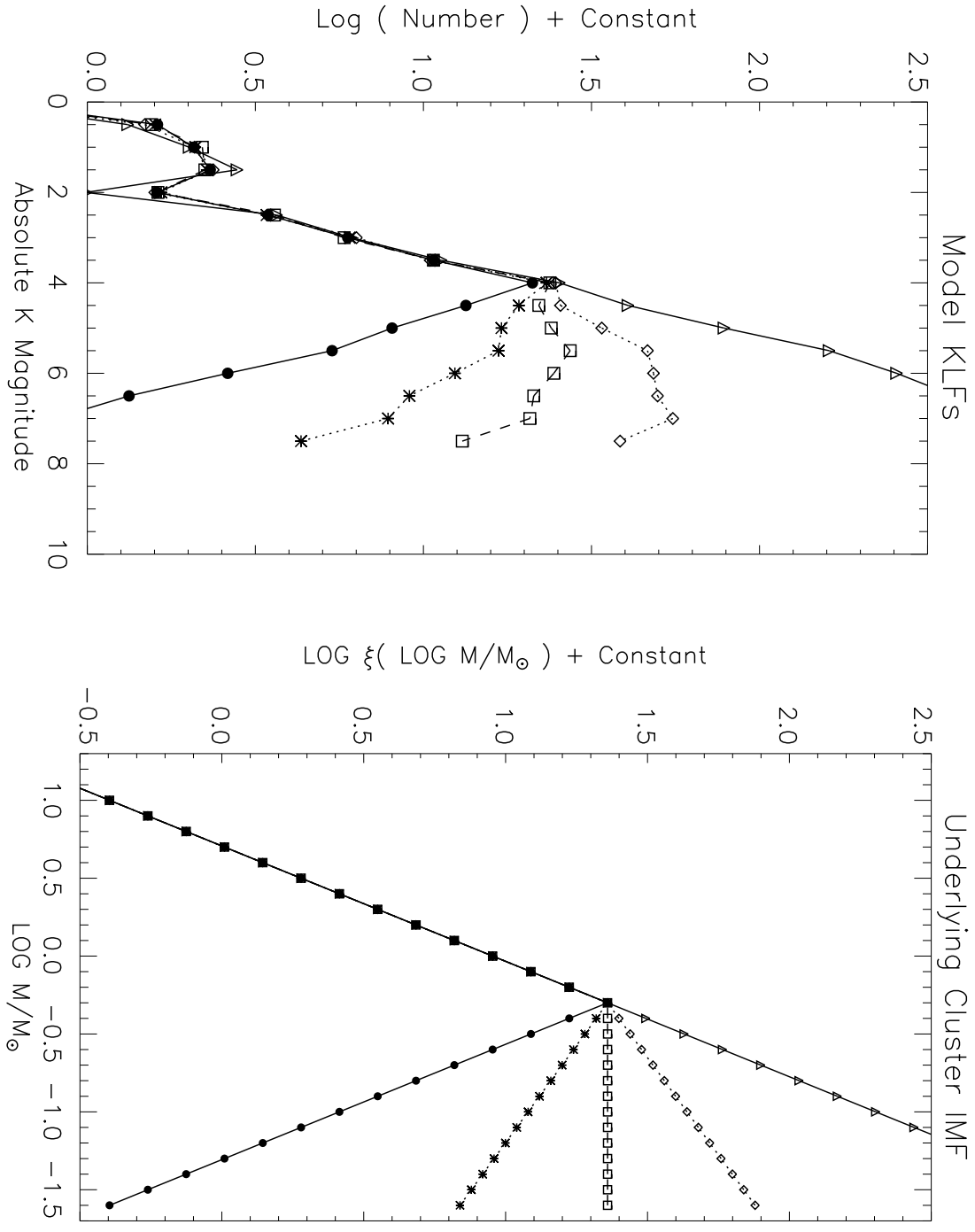
Model KLFs
Log (Number) + Constant
Absolute K Magnitude
Underlying Cluster IMF
LOG ξ(LOG M/M⊙) + Constant
LOG M/M⊙

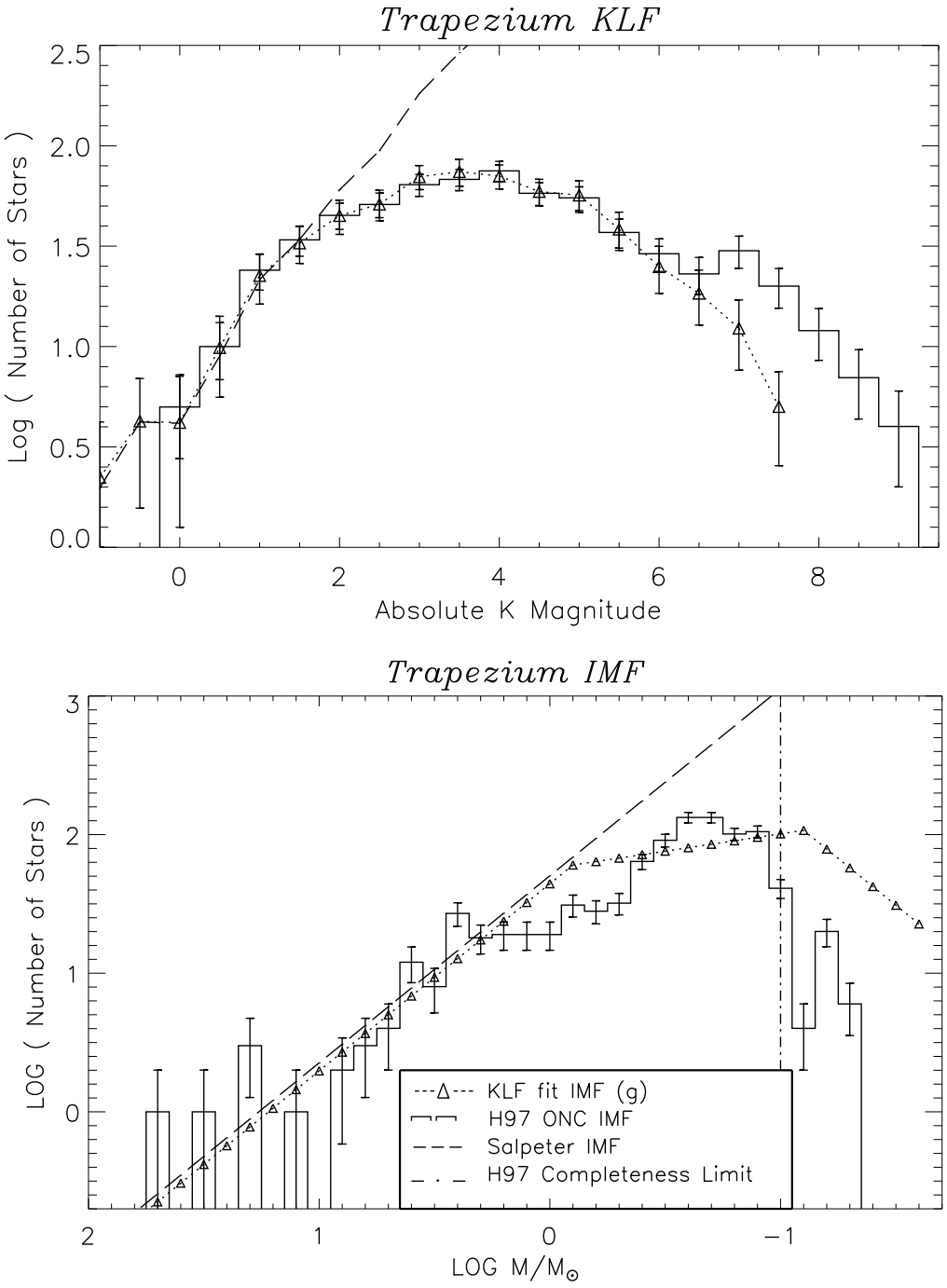
Trapezium KLF
Log (Number of Stars)
Absolute K Magnitude
Trapezium IMF
LOG (Number of Stars)
LOG M/M⊙
KLF fit IMF (g)
H97 ONC IMF
Salpeter IMF
H97 Completeness Limit